Article

Novel FPGA-Based Visual Stimulation Method for Eye Movement Analysis

Alejandro Benitez Fernandez [1,*], Bárbaro N. Socarrás Hernández [2], Justo M. Herrera Rodríguez [2], Bruno da Silva [3] and Carlos R. Vázquez-Seisdedos [2]

[1] Department of Telecommunications, Universidad de Oriente, Santiago de Cuba 90500, Cuba
[2] Center for Neuroscience Studies, Image and Signal Processing, Universidad de Oriente, Santiago de Cuba 90500, Cuba; bnshdez248@gmail.com (B.N.S.H.); justicohr@gmail.com (J.M.H.R.); cvazquez@uo.edu.cu (C.R.V.-S.)
[3] Department of Electronics and Informatics, Vrije Universiteit Brussel, 1050 Brussels, Belgium; bdasilva@etrovub.be
[*] Correspondence: benitez6000@gmail.com

Abstract: Several studies have demonstrated that irregularities in eye movements represent an important indicator to diagnose diseases affecting the central nervous system. In fact, abnormal horizontal and vertical eye movements play an important role in measuring the progress of neurodegenerative diseases. Electro-oculography (EOG) is a widespread technique that monitors the horizontal and vertical eye movements in response to a visual stimulation pattern. These visual stimuli require stimulus-response synchronization, low latency, and a real-time response. In this work, a novel system based on a Field-Programmable Gate Array (FPGA) is designed to address hundreds of LEDs for the generation of multiple visual stimulus signals and for EOG acquisition. Our evaluation demonstrates that the proposed system enhances the accuracy of the signals generated, showing excellent results in the stimulus-response synchronism and quality of the stimuli waveform.

Keywords: electrooculography; visual stimulation; eye movement analysis; neurodegenerative diseases; FPGA

1. Introduction

Eye movement analysis has vital importance in the diagnosis of illnesses related to the central nervous system (CNS). An electro-oculogram allows the registration of the corneo-retinian potential using electrodes placed in the eye's vicinity. The resulting signal is denominated by an electro-oculographic (EOG) signal [1], which is used for multiple applications, standing out especially in marketing and medicine. In the latter, its use in real-time eye-tracking systems stands out as a human–computer interface (HCI) for disabled people [1,2]. Nonetheless, EOG are mostly used for the diagnosis of diseases. The use of patterns for visual stimulation and their corresponding eye biological response signal allows for diagnoses of damage to the vestibular system [3,4], ataxia [5,6], cerebellar pathologies and diffuse encephalopathies [7], schizophrenia [8,9], autism [10], Alzheimer's Disease [11], Parkinson's Disease [6], amyotrophic lateral sclerosis [12], aging [13], and drug consumption [14]. Moreover, eye movement disorders constitute an early indicator for diagnosis of these diseases. Visual stimuli generation methods for the diagnosis of neurodegenerative diseases using EOG are insufficiently addressed in the literature. Very few research papers propose visual stimulators based on EOG signals [15,16]. The presented work intends to extend this application of EOG by proposing a system designed for the diagnosis of neurodegenerative diseases.

The visual stimulus signal and its relationship with the ocular signal is very important for diagnosis. One of the main parameters to analyze in the design is the synchronous acquisition of the visual stimulus and the EOG signal from the patient. This parameter

facilitates to evaluate the latency of the patient's visual response to a given visual stimulus. This parameter is critical, being an early indicator of several neurodegenerative diseases, such as Parkinson's [17], amyotrophic lateral sclerosis [18], and Friedrich's ataxia, the latter being of high incidence in Cuba [19]. The literature indicates that latency times for healthy people are lower (typically 200 ms) than in people suffering from these diseases (around 300 ms), and this imposes a condition on the designed system. Hence, an EOG system for diagnosis of neurodegenerative diseases must offer low latency and a fast response, among other characteristics.

Field-Programmable Gate Arrays (FPGAs) have well-known advantages when used on embedded systems. They not only offer high power efficiency, but also low latency and high performance, which make them ideal candidates for a complex visual stimulator. The computational power and storage capacities of FPGAs guarantee the synchronism between stimulus-response signals and efficiency for a system controlling hundreds of LEDs used for visual stimulation. Lastly, their flexibility grants the custom stimulus a pattern design and performance for patients with special needs. To our knowledge, there is no evidence in the literature of the use of an FPGA-based method for the visual stimulation of patients with neurodegenerative diseases using EOG.

The main contributions of this paper are:

- Design of a visual stimulation novel method for EOG systems using the advantages of parallelism, hardware, and the processing speed of FPGAs.
- Design of a reconfigurable system with a multiplicity of stimuli generation, along with synchronism between the stimulus signal and the EOG signal acquisition.

This paper is organized as follows. In Section 2, the work related to visual stimulators is discussed. Section 3 describes the background of the system, the signals generated, and the general architecture of the visual stimulation and EOG signal acquisition system, based on FPGA. In Section 4, our system is described, along with the proposed method for the generation of visual stimuli. Section 5 explains the evaluation methodology, and deploys the obtained results. In Section 6 the results and flexibility of the system are evaluated and compared to other research papers in the literature. Finally, the conclusions are drawn in Section 7.

2. Related Work

The work related to visual stimulators can be classified in patents, commercial equipment, research projects that propose visual stimulators for applications related to the brain–computer interface, and those using visual stimulation in conjunction with EOG for the diagnosis of certain diseases.

In the last 20 years, there have been very few publications that address the design of visual stimulators, although there is a variety of EOG equipment on the market [20,21]. Most of the related work use commercial equipment to perform eye signal analysis. In the Refs. [22,23], mirror galvanometers were used for stimulation to provide evidence of the synergy between saccades and pursue movements under certain conditions. The stimulus consists of a green fixation dot and a set of red dots that are moved on the horizontal axis by the galvanometer. The subjects have to pursue the red stimulus with their gaze following an ellipsoidal path with a horizontal amplitude of 20° and vertical amplitude of 10° at a frequency of 0.195 Hz. In the Ref. [24], the BM 6000 Ganzfeld (Biomedica Mangoni, Pisa, Italy) was used to analyze electroretinography signals and oscillatory potentials for the diagnosis of CADASIL disease [25] using a CRT monitor as a stimulation panel. For the tests, patients were stimulated with saccades of 5 ms at a frequency of 0.1 Hz. Similarly, the authors in the Ref. [26] used an AMTech Digital LED Bar 96 (AMTech GmbH, Weinheim, Germany) to stimulate schizophrenic siblings. The patients were stimulated with four visual stimuli, while the EOG response was recorded using infrared oculography. In the Ref. [27], an eye tracking device manufactured by SensoMotoric Instruments (SMI) was used for the analysis of saccadic eye movements under a double-step paradigm for ocular analysis. Visual stimuli consist on solid white dots (4 mm in diameter) on a gray

background displayed on a screen. This system has proprietary software for stimulation and signal acquisition that generates ±5°, ±10°, and ±20° saccadic signals.

The main disadvantage of using the above commercial devices is that they do not allow customized stimuli and tests, since they constitute black boxes with unknown internal functioning protected by commercial rights. Furthermore, research projects using them have the limitations of high cost and low flexibility in their systems. Important parameters, such as the latency of the system and the stimuli waveform generation methods are unknown, hence, they were not analyzed in those research papers.

Most novel visual stimulators target visual research applications and the brain–computer interface (BCI). In the Ref. [28], a design of a low-cost, portable, and micro-controlled visual stimulator was proposed. Unlike previous ones, this system allows the connection of up to nine LEDs for visual stimulation, which are managed independently. Its performance has been tested in the acquisition of evoked potentials, using a single stimulation channel. Its main limitation, in our consideration, is that it does not have an interface with the PC, which makes it a very inflexible system, in addition to being designed only for evoked potential systems. Visual stimulators for similar applications were designed by the Refs. [29,30], the former using an FPGA to generate the visual stimuli for evoked potentials on an LCD monitor. The system proposed In the Ref. [30] uses two arrays of five LEDs located at 5° from the center of the patient's visual field to generate visual stimuli that provoke evoked potentials for the development of a new paradigm for studying the individual's spatial selective attention.

The described systems are relatively simple visual stimulators. Although they use the same patterns used for EOG, only single or a pair of LEDs compose their system. Moreover, the biological signal obtained from the stimulus is not an eye signal, but a brain signal. Hence, they cannot be used for the diagnosis of neurodegenerative diseases.

In the Ref. [16] the authors designed a system for the diagnosis of ocular dysfunctions where the Retinal Pigment Epithelium is damaged. The system uses an FPGA for stimulation and acquisition of the signals. This system consists of placing three LEDs inside the dome (a kind of helmet) located in front of the patient; one white LED at the 0° position, and two red ones at ±15° related to the patient's field of vision. The stimuli consist of turning on the LEDs alternately at a frequency of 1 Hz. Despite the use of an FPGA, the visual stimulator is relatively simple, mainly since it is designed for the diagnosis of eye diseases; hence, it only has one type of stimulus and does not analyze stimulus-response latency because the application does not require it.

Regarding the design of a visual stimulator as part of an electrooculographic system for the diagnosis of neurodegenerative diseases, we only found the work of Perez Guzman [15]. This paper designs a system to visually and auditorily stimulate patients suffering from Spinocerebellar ataxia type 2 in Cuba. It has the advantages of using the Arduino platform, which makes the addition of new functionalities more flexible. Furthermore, it is presented as a low-cost solution, although it does not perform a detailed cost analysis of the design. In our consideration, the design has the drawback of using a TV set as a stimulation panel, which is counterproductive with the portability and low costs that the authors attribute to the design. The system uses four microcontrollers (two Arduino boards, the PC and a TV set), hence there will be inevitably certain delays in signal transmission. On the other hand, they do not specify the characteristics of the two stimuli used (amplitude, frequency, waveform) or how they are generated; thus, they do not perform a deep evaluation of them. Finally, the system is made for substitution of electronystagmography equipment; hence, it inherits their main characteristics and limitations.

There is limited literature on the design of visual stimulators as part of EOG systems. Most of the proposed designs focused on BCI applications, without performing a deep quantitative analysis of the characteristics of the stimuli. Similarly, most of the designs of visual stimulators as part of EOG systems do not analyze important parameters, such as stimulus-response latency. In addition, they do not have flexibility in the generation of multiple visual stimuli. The presented work intends to fill this gap by presenting a

novel architecture for diagnosis of neurodegenerative diseases using a visual multi-stimuli system for EOG.

3. Background

For detecting potential neurodegenerative diseases using EOG, there are different types of visual stimuli. Analyzing their principles and characteristics is important to understand the architecture of the proposed system.

3.1. Visual Stimulation

The stimulus can be displayed on a panel of LEDs or on a Cathodic Rays Tube (CRT) monitor or Liquid-Crystal Display (LCD) monitor. Depending on the display selected, the methods for generating the signals are less or more complex. Monitors allow for a higher resolution in the stimulus generation, and their main drawbacks are power consumption and portability. On the other hand, the LED panels are the counterpart of the previous ones, and they have an acceptable resolution, but at lower costs and with great portability. Furthermore, they do not cause significant electromagnetic interference on the EOG signals [31], and due to this nearly instantaneous switching response [32], they are ideal for complex displays and finely controlled temporal patterns of stimulation. Therefore, this is the panel stimulation utilized in this research.

The setup for the visual stimulation is depicted in Figure 1. The patient must be located at a distance (D) from the visual stimulator. The value of D ranges from 30 cm to 200 cm, which is used together with the distance from the centre to the extremes of the visual stimulator (W) to calculate the angle of ocular movement (λ).
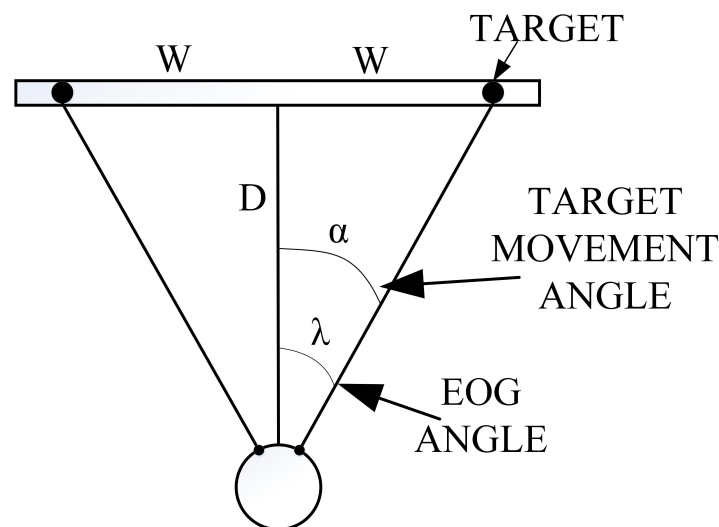
Figure 1. Relation among the width (2W) of the screen, the distance (D) of the patient, and the maximum angle of vision (2α).

The angles of target movement (α) and ocular movement (λ) must be the same. A difference between them is not desirable for the correct diagnosis. The latter could happen when there are head movements during the tests, which can provoke failures in the diagnosis.

The relation between D, W, and the angles to perform different visual stimulations is expressed by Equation (1).

$$tan\ \alpha\ =\ \frac{W}{D} \tag{1}$$

The most frequently used patterns for visual stimulation in patients with neurodegenerative diseases are saccades and smooth pursuit signals [1,27,33].

3.1.1. Saccadic Stimuli

A simple saccadic (SSAC) stimulus is a type of visual stimulation where a point (in our case, a lit LED) appears in a position on the screen and stays illuminated for a certain time. It then disappears and appears in another position by activating another LED on the same horizontal axis. To follow the point with the gaze, the patient must perform a saccadic movement in order to focus on the new position of the point each time it changes. Figure 2 shows an example of a stimulus and the corresponding EOG response acquired in the horizontal lead (EOGH) for a healthy patient.
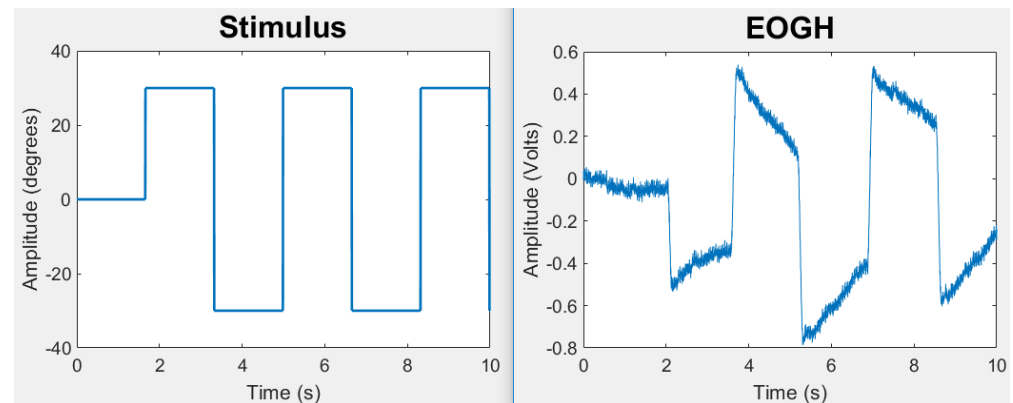
Figure 2. Example of a saccadic stimulus signal (**left**) and the EOG response acquired in the horizontal lead (**right**).

In a system using LEDs, the stimulus consists of turning on a single LED at a given moment in time. The direction and speed of the LED light on the horizontal axis will shape the stimulus signal. By switching specific LEDs on and off, the left signal in Figure 2 can be achieved. The edges of the stimulus signal in Figure 2 represent the changes of position in the light signal on the horizontal axis, while the flanks in the response signal represent the saccades from left to right (rising edge) and from right to left (falling edge) made by the oculomotor system.

The literature provides evidence of the EOG having precision below 2°, and the signal can be considered linear for gaze angles of up to ±30° [1], which means changes in the stimulus cause equal angular increases in the EOG signal. Hence, this value is generally considered the maximum for a saccadic test [1,33,34], and multiple authors choose ±10° and ±20° as typical values [27,35,36].

The distance between the patient and the stimulus (D) is an important factor because the stimulus must be clearly visible, even for patients with vision problems. In this regard, the bibliography is not very precise, but the values vary between 30 cm [37], 50 cm [38], 75 cm [24], 83 cm [36], 90 cm [39], 100 cm [40], 120 cm [41], 150 cm [42], 170 cm [22], and 200 cm [26].

The frequency of the saccadic stimulus is of utmost importance. Patients who are under a test usually have problems in the oculomotor system, such as high latencies and low saccadic velocity. Regarding this aspect, the literature shows the ranges of these values are between 0.1 Hz and 1.1 Hz, with a resolution of 0.1 Hz [27,34,36], taking typical values for the tests 0.2 Hz and 0.3 Hz. For instance, the stimulus in Figure 2 shows the SSAC stimulus consists of a rectangular pulse train. This signal only has two states, meaning that only two LEDs are lit during the test, the maximum and the minimum. Equation (2) relates the LED lighting time regarding the frequency of the saccadic stimulus, where t_{SSAC} represents the time each LED is lit, and f_{STIM} represents the stimulus frequency.

$$t_{SSAC} = \frac{1}{2 \times f_{STIM}} \tag{2}$$

Under certain conditions, patients may predict the stimulus position during tests, and therefore, they introduce a bias. If that is the case, the random saccadic (RSAC) stimulus can be used. Although the same parameters of the conventional saccadic test follow (even the same equation), its main difference resides in the use of pseudorandom stimulus amplitudes, impelling the patient to predict the stimulus position.

3.1.2. Smooth Pursuit Stimuli

Smooth pursuits are a different type of visual stimuli. The stimulus on these tests moves on the horizontal axis describing a linear (Smooth Pursuit with Constant Speed, SPCS) or sinusoidal (Smooth Pursuit with Sinusoidal Speed, SPSS) law, causing the patient to follow it through slow movements of their eyes. An example of a SPSS signal corresponding to the stimulus (left) and the EOGH response of a healthy patient (right) are shown in Figure 3.
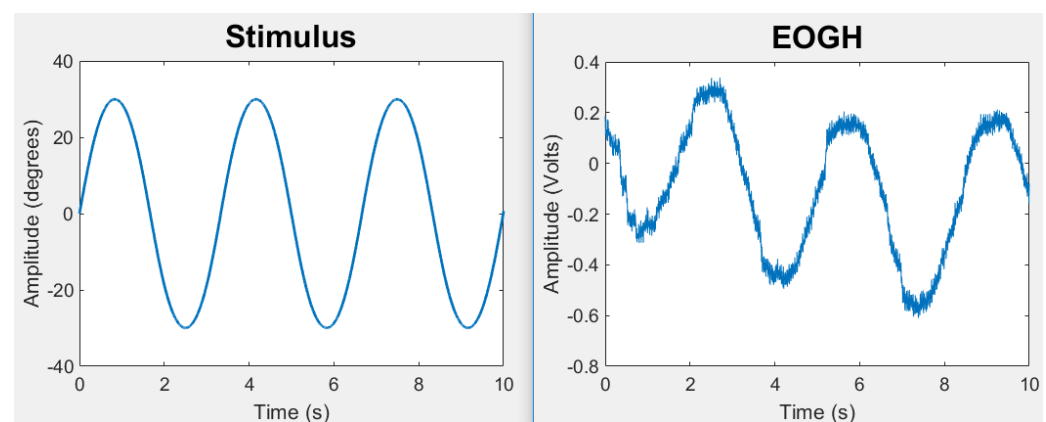
Figure 3. Example of a SPSS stimulus signal (**left**) and the EOG response acquired in the horizontal lead (**right**).

The generation of smooth pursuit stimuli on systems composed of multiple LEDs is done by lighting the LEDs consecutively following a linear (SPCS) or sinusoidal (SPSS) equation. Only one LED is lit at a time, and the change in the signal amplitude is seen by the patient as a single luminous dot (a lit LED) moving in the horizontal axis.

The stimuli frequency is of utmost importance because the patients under test generally present problems in the ocular-motor system, such as high latencies and low ocular speed. The literature shows the ranges of these values are between 0.1 Hz and 1.2 Hz, with steps of 0.1 Hz [23,27,34,36,43], taking as typical values for the tests 0.2–0.4 Hz. However, there are other studies that stimulate at a higher frequency [39,44].

Regarding the duration of the stimulus, related work often consider smooth pursuit tests with a maximum duration of 50 seconds [40]. After this time, the patient loses concentration and/or experiences ocular fatigue.

Smooth pursuit with constant speed signal.

Although the previous visual stimulus only presents variations on the horizontal axis, the visual stimulus can also be bi-dimensionally generated using a linear array of LEDs. For instance, a SPCS stimulus signal depicted in Figure 4 has a triangular signal. This example is a symmetrical signal with odd parity, hence the pendent of all its sections is the same. Figure 5 shows how the patient perceives this visual stimuli on the panel of LEDs. The different stages of the triangular signal shown in Figure 4 corresponds to the perceived changes in the LED activation pattern shown in Figure 5.
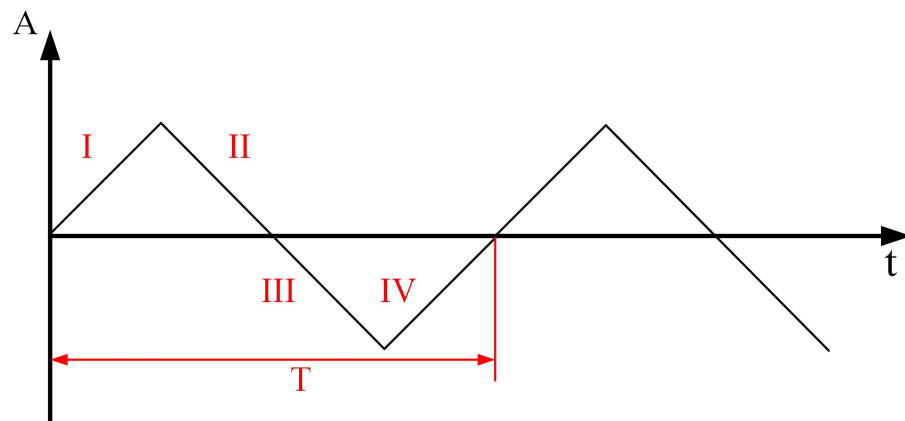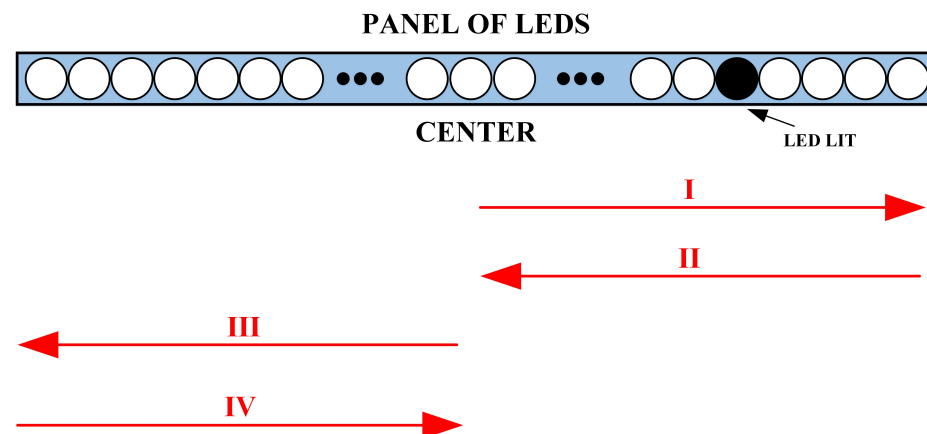
Figure 4. SPCS stimulus signal.

Figure 5. SPCS signal visualization pattern in the panel of LEDs for the triangular signal depicted in Figure 4.

On the other hand, to obtain each LED lighting time for the SPCS (t_{SPCS}), it would be required to only analyze one of the signal sections. Equation (3) is obtained by knowing the total amount of LEDs needed from left to right for the maximum amplitude (A_N) and the stimulus frequency (f_{STIM}).

$$t_{SPCS} = \frac{1}{2 \times A_N \times f_{STIM}} \tag{3}$$

Smooth pursuit with sinusoidal speed signal.

The SPSS signals are a different type of smooth pursuit stimuli that consists of a symmetrical sinusoidal signal regarding the panel of the LED center. Similarly, for SPCS, the bi-dimensional pattern of the SPSS can be generated using the linear array of LEDs. Performing the same analysis made for the SPCS signal, Equation (4) describes the time that should be a LED lit for a sinusoidal stimulus.

$$t_{SPSS} = \frac{sin^{-1}\left(\frac{2 \times A_i}{A_N}\right)}{2 \times \pi \times f_{STIM}} \tag{4}$$

where A_i represents the analyzed LED in a time instant. Contrary to the previous signal, the SPSS signal has as many t_{SPSS} values as LEDs have tests, fundamentally due to the variable speed of a sine wave; therefore, the LED lighting times are not equal to the same test.

Table 1 summarizes the stimulus characteristics used in the implemented system.

Table 1. Stimulus summary.

Stimulus	Notation	Characteristics	LEDs Ligthing Time
Simple SACcadic	SSAC	The stimulus abruptly jumps between two positions in the horizontal axis.	$t_{SSAC} = \dfrac{1}{2 \times f_{STIM}}$
Random SACcadic	RSAC	The stimulus pseudo-randomly jumps among several positions in the horizontal axis	$t_{RSAC} = \dfrac{1}{2 \times f_{STIM}}$
Smooth Pursuit with Constant Speed	SPCS	The stimulus moves on the horizontal axis describing a linear law	$t_{SPCS} = \dfrac{1}{2 \times A_N \times f_{STIM}}$
Smooth Pursuit with Sinusoidal Speed	SPSS	The stimulus moves on the horizontal axis describing a sinusoidal law	$t_{SPSS} = \dfrac{sin^{-1}\left(\frac{2 \times A_i}{A_N}\right)}{2 \times \pi \times f_{STIM}}$

4. Platform Description

This section explains the insides of the proposed system. Firstly, a general description detailing the functionality and the support for the visual stimulus is provided. Secondly, the different stages of the system are described in detail.

4.1. General Description

Multiple electrodes are placed in the face of the patient in order to capture the EOG signal, as depicted in Figure 6. The medical staff working in the desktop PC sends, through USB communication, a data transfer with the characteristics of the tests. A USB controller manages the communication between the desktop PC and the CM block on the FPGA, which receives the data from the PC and sends it through four 8-bit frames or commands to the SG. Based on the command received, the SG obtains the information related to the LED's lighting time and the position in the array of the active LED. An output signal corresponding to the position of a specific LED in the array is generated to activate the LED. The same output signal, which constitutes the stimulus, is sent to the PM, also responsible for building an 8-byte multi-frame with the stimulus and EOG signal from the patient and sending it to the PC. Both signals, stimulus and response, are sent in the same frame, which grants a real-time response.

The proposed system is designed to support up to six stimulus amplitudes (±5°, ±10°, ±15°, ±20°, ±25°, ±30°) and 12 stimulus frequencies (0.1 Hz–1.2 Hz) with a resolution of 0.1 Hz. The considered patient-stimulus distances (D) are 50 cm and 100 cm.

The proposed system is composed of three main stages (Figure 6):

- **Visual Stimulator**: In this stage, the visual stimulus is generated. It is composed of an external stimulus panel (SP) controlled by the stimuli generator (SG) implemented on the FPGA.
- **EOG Acquisition**: This stage is in charge of capturing and processing the patient's ocular movements. It is composed of an external EOG amplifier and a packaging module (PM) running on the FPGA.
- **Communication and Power Management**: This stage includes the Communication Module (CM) on the FPGA and a USB controller for the communication with PC managed by the medical staff controlling the patient's test. Additionally, the power source for the system is represented.

Although the system used external components such as the SP, the core of the proposed system is implemented on the FPGA. The components allocated on the FPGA are the SG,

the PM, and the CM, which belong to the Visual Stimulus, the EOG Acquisition, and the Communication stages, respectively.
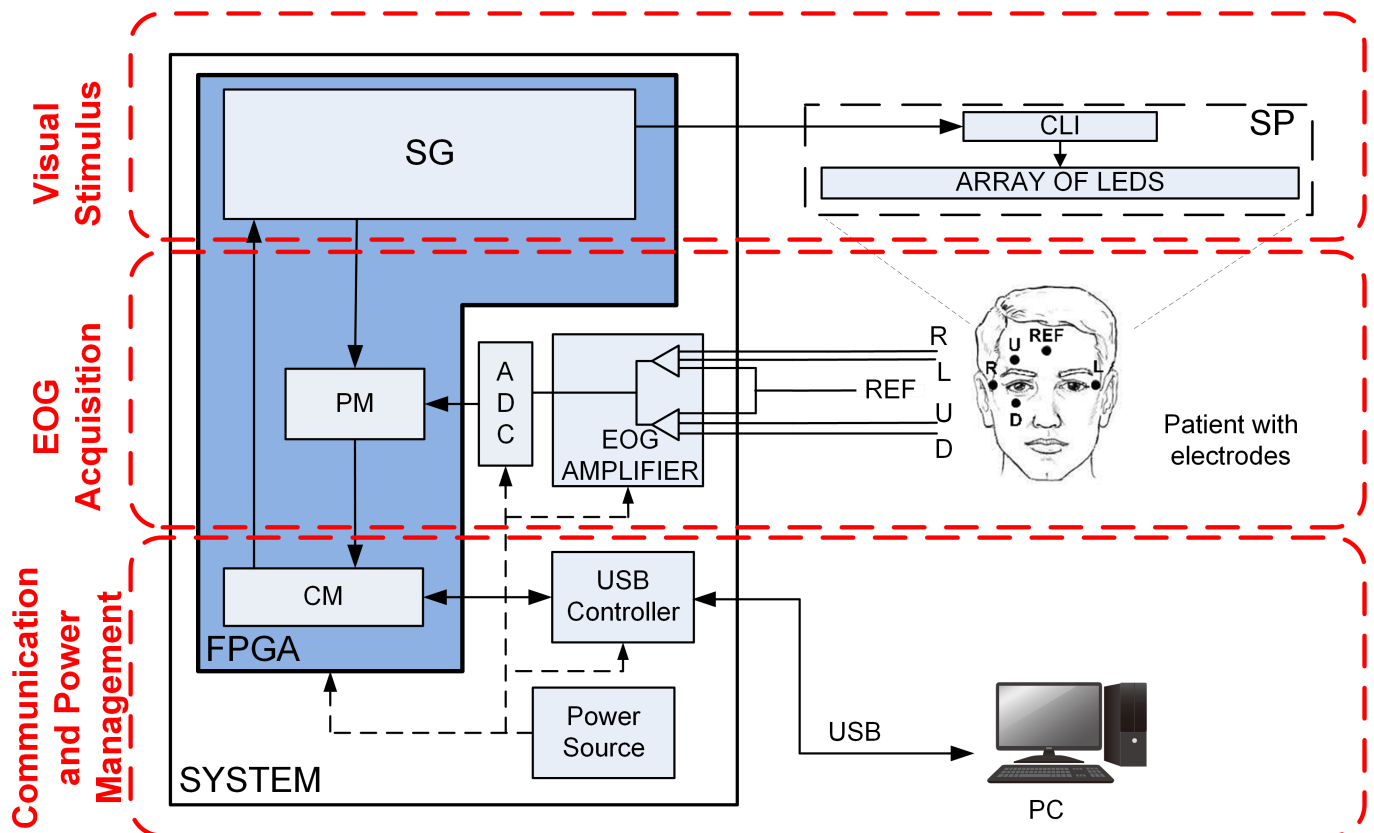

Figure 6. Blocks outline of the general system.

4.2. Visual Stimulator

4.2.1. Stimulus Panel

The parameters for the design of the SP are the distance D and the diameter of the LEDs (d). Equation (5) relates Equation (1) with *d*, where A_N represents the number of LEDs that need to be lit for a given stimulus.

$$A_N = \frac{2 \times (D \times tan\ \alpha)}{d} \qquad (5)$$

For the sake of visibility, commercial LEDs with d equal to 5 mm can be assumed to be placed without spaces between them. Hence, for a test of 30° and D = 100 cm, it is necessary to turn on 236 LEDs, which constitutes the maximum number of LEDs of the SP.

As shown in Figure 7, a Combinational Logic Interface (CLI) is used for decoding the 8-bit signal from the SG to address the 236 LEDs of the SP.

To handle the array of LEDs, 31 lines are needed. Thus, the array is considered a matrix for addressing purposes. As can be seen in Figure 7, the LED cathodes are connected in groups of 16 to the bottom decoder outputs. In these groups, each anode is connected to an output of the other decoder through an inverting gate and a resistance. By selecting a specific output of each decoder, any LED in the array can be activated.

The use of the CLI inserted on the SP has the advantage of wire simplicity. Only 8 wires from the FPGA to the SP are needed for addressing the LEDs. As a result, the system is less bulky and allows the use of low-end FPGAs offering a low number of general-purpose inputs/outputs (GPIO).
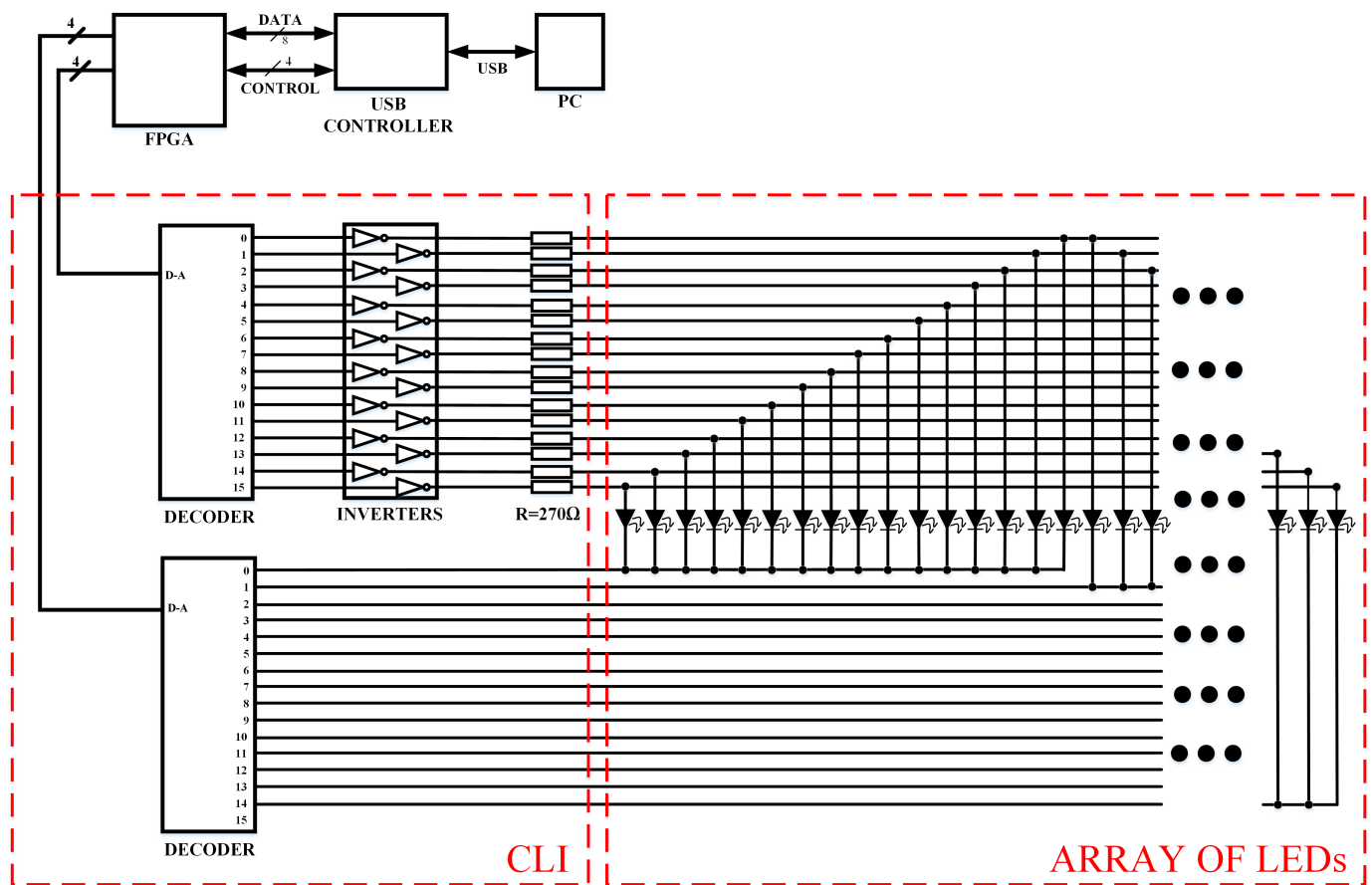
Figure 7. Details of the Combinational Logic Interface (CLI) to address the LEDs in the Stimulus Panel.

4.2.2. Stimuli Generator

Figure 8 details the blocks outline of the stimulator. The SG includes: (a) a transcoder that identifies and separates the bytes with the information of the stimulus, (b) a Phase Locked Loop (PLL) that generates a clock signal of 1 MHz for the internal blocks, (c) six Read-Only Memories (ROM), four containing the lighting time values of each LED, where the fifth stores the random saccadic test amplitudes, and the last one, the amplitudes of the other tests, (d) six signal generators to fill the ROM, (e) a control unit for managing the process of visual stimulation, and (f) a multiplexer that selects the stimulator output depending on a logic that considers the characteristics of the test to perform.

Figure 9 represents a Finite State Machine (FSM) of the novel method designed for generating the visual stimuli inside the FPGA.

In the START state, the system initializes by generating and storing in the internal FPGA memory (ROMs) the tables with LED lighting times and their positions in the SP. Then, the SG passes to the PAUSE state. It will only leave this state when it receives from the PC the characteristics of a test (amplitude, frequency, distance and type of stimulus) along with the command to initiate a test. In that case, the SG automatically reads from the ROMs the initial LED lighting time and its position in the SP (ROM READING state). Then in the VISUAL STIMULUS state, the LED position to the array of LEDs is sent through the CLI. The time the LED will be lit is the LED lighting time read in the previous state. When this time is consumed, the system returns to the ROM READING state. It will alternate between this state and VISUAL STIMULUS until it receives the command for ending the test, and then it passes to the PAUSE state.
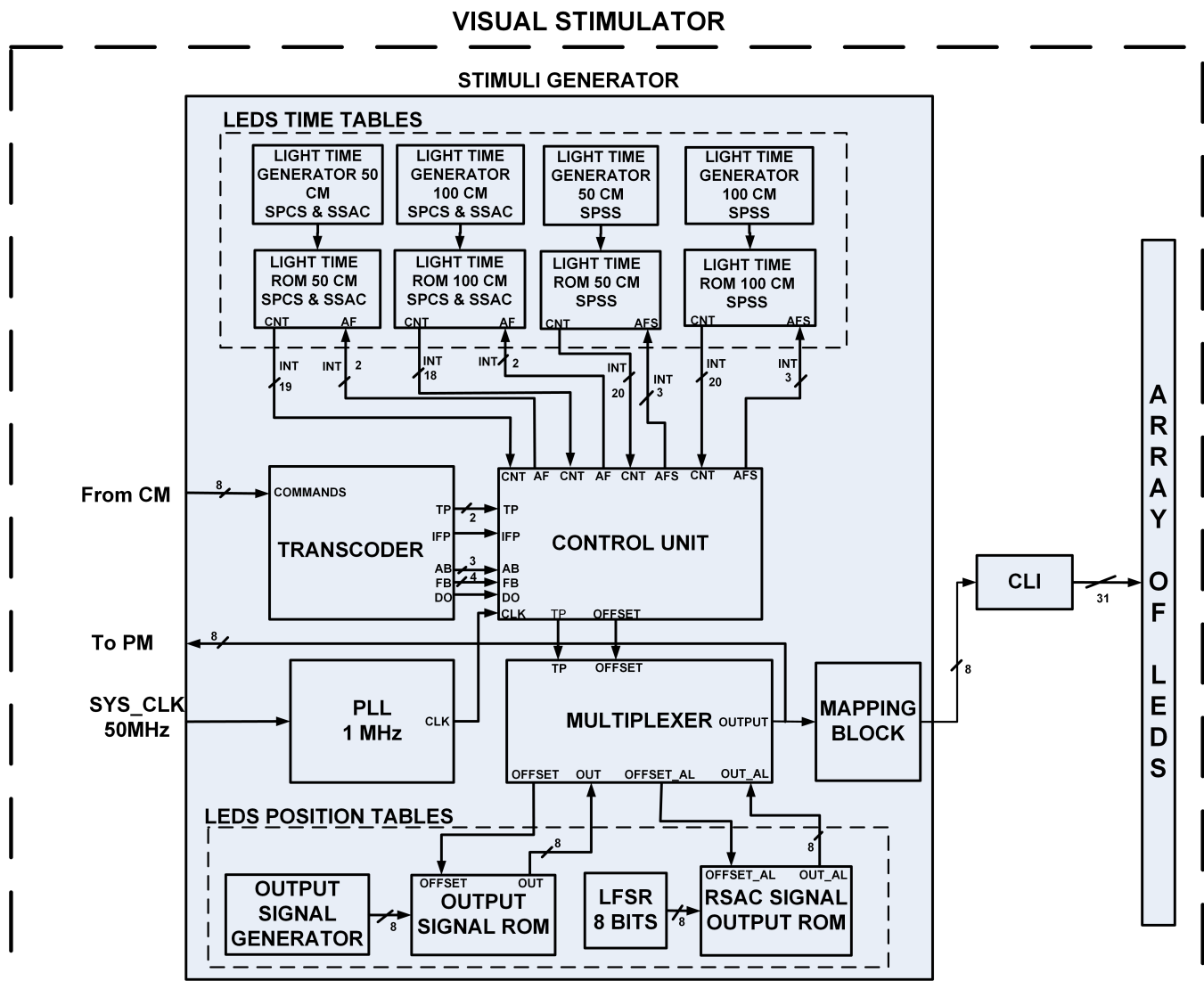
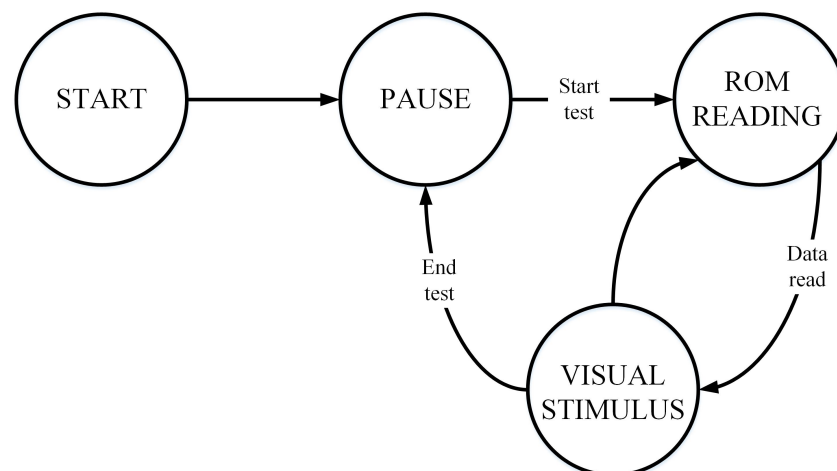**Figure 8.** Blocks outline of the stimulator.

Figure 9. States of the Stimuli Generator (SG).

4.2.3. LED Time Tables

The SG is conditioned by the characteristics of the supported stimulus. There are two parameters whose control is fundamental: the lighting time of each LED and the

addressing of their positions in the array. The first one is the most complicated to handle, since there are four possible tests with two supported distances between the patient and the stimulus, with six possible values of α, 12 frequencies, and 236 LEDs. Hence, there are at least 14,112 time values for each test in the worst-case scenario where each LED has a different lighting time.

The generation of the SSAC, RSAC, SPCS, and SPSS signals is carried out by implementing Equations (2)–(4), respectively. These equations detail how long an LED should be on in the LED array. The consecutive lighting of the different LEDs gives the waveform to the stimulus signal.

SPCS, SSAC and RSAC signals.

In the SPCS signal there will be as many t_{SPCS} as combinations of amplitudes and frequencies for each distance D. The signal has a linear behavior and therefore, in a test, all the LEDs will have the same lit time. Thus, there will be 72 t_{SPCS} for each distance D.

An analysis on the SSAC signal demonstrates that it can be generated through the t_{SPCS}. Equation (6) relates it.

$$t_{SSAC} = t_{SPCS} = \frac{1}{2 \times A_N \times f_{STIM}} \tag{6}$$

Equation (6) can be transformed into Equation (2) when $A_N = 1$, meaning that during a SSAC test only a LED must be lit in each section of the signal. Therefore, it allows the same generator to be used for both signals.

Although LED lighting times should be expressed using floating-point values, the floating-point representation would lead to unnecessary resource consumption and performance reduction. Instead, integer values are used. The integer types conversion is done using the PLL. Equation (7) shows this process for the SPCS signal.

$$count_{SPCS} = t_{SPCS} \times f_{PLL} \tag{7}$$

where $count_{SPCS}$ represents the integer of each LED lighting time and f_{PLL} represents the PLL frequency. These counts are stored in two-dimensional ROMs for the SPCS and SSAC signals (Figure 10).
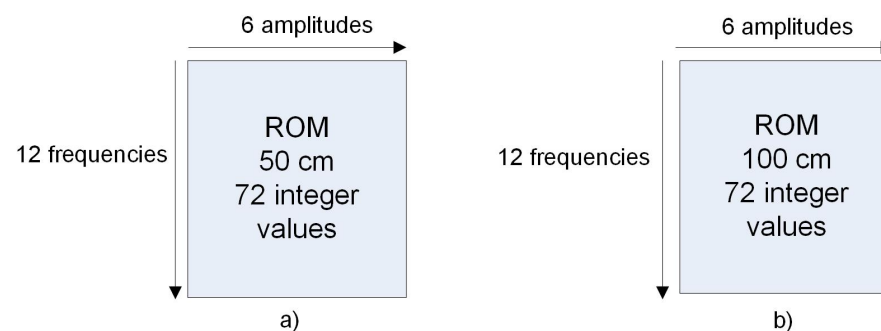
Figure 10. Storage of LED lighting times. ROMs with 144 values (72 each) for the SPCS and SSAC tests for (**a**) 50 cm and (**b**) 100 cm.

The RSAC signal, as stated in Section 3.1.1, uses the same parameters regarding LED timing as the SSAC signal. Therefore, there is no need to create a new ROM for storing these LED lighting times.

SPSS signal.

Equation (4) relates the lit times of the LEDs in the SPSS signal. Being a sinusoid, its rate of change varies following a cosinusoidal law. Therefore, unlike the two previous signals, in every signal section, each LED lights up a different time with respect to the others. This means that for a test, there are as many t_{SPSS} as LEDs.

Analyzing the SPSS signal characteristics (Figure 11), it is observed that a period can be divided into four sections, where it is evident that between sections I and II, and III and

IV, respectively, there is an even symmetry, and between sections I–II and III–IV, there is odd symmetry. Therefore, knowing the above, it is only necessary to calculate and store the LED lit times of section I, as these will be the same for the rest of the sections.
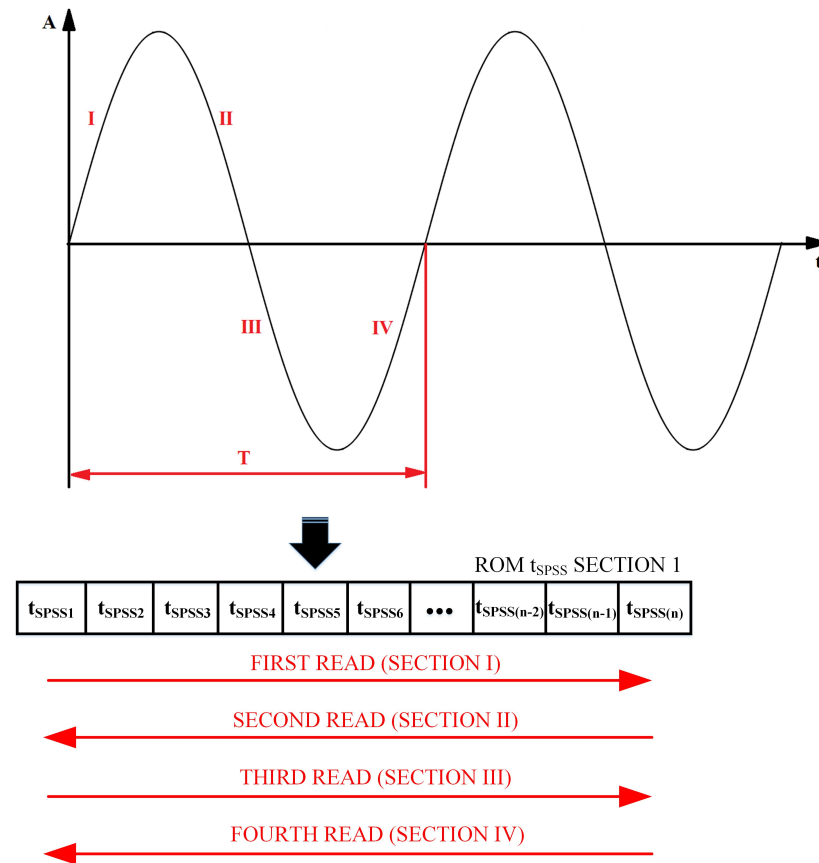
Figure 11. Reading procedure for the SPSS ROM.

The same procedure is done to store the t_{SPSS} as for the SSAC and SPCS signals using the f_{PLL}. However, in the SPSS signal, for each combination of amplitude and frequency there will be $A_N/4t_{SPSS}$ (Figure 12). Hence, for storing the LED lighting times of the SPSS signal, the use of three-dimensional ROM is needed.
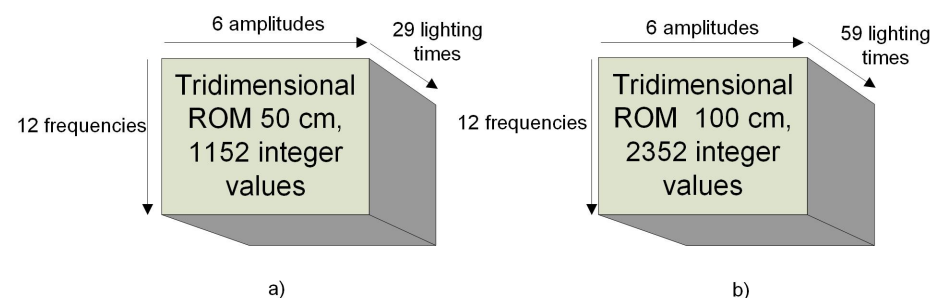
Figure 12. Storage of LED lighting times. Tri-dimensional ROMs for the SPSS tests of (**a**) 50 cm and (**b**) 100 cm.

Storing only the first quarter of the SPSS signal allows to save storage space, creating a more efficient system.

4.2.4. LED Position Tables

The SG also generates the possible values the output signal has towards the CLI. These values correspond to the 236 LEDs on the array. The output signal from the Multiplexer to

the CLI is mapped. This allows the decoders in the CLI to sequentially address the LEDs in the array.

SSAC, SPCS and SPSS signals.

For the SSAC, SPCS and SPSS tests the SG and generates an 8-bit signal which allows to address all the LEDs on the array. It is a binary count of 236 states, thus the SG has a block, which is a binary counter. In consequence, to turn on LED 1 of the array, the binary code "00000001" will be sent to the CLI and so on until LED 236 is switched on, which corresponds to the code "11101100". The generated output signal is stored in a ROM of 236 positions, and each value corresponds to the position of a LED in the array, hence the memory stores 236 bytes.

RSAC signal.

The RSAC test prevents the patient from predicting where the stimulus will be found in the LED array at a given time. To achieve it, a signal with pseudo-random values must be generated. The method chosen for its implementation is using a Linear Feedback Shift Register (LFSR) and storing its values in a ROM.

The LFSR is a shift register in which the input is a bit from applying a linear transformation function (usually a polynomial) to an earlier state. The initial value is called the seed, and the sequence of values produced by the register is completely determined by the current or previous state of the system. The sequence generated has a repetition period, which is generated again after all possible states and repeated indefinitely. A conventional LFSR or 8-bit Fibonacci LFSR is chosen. Figure 13 illustrates this type of shift register.
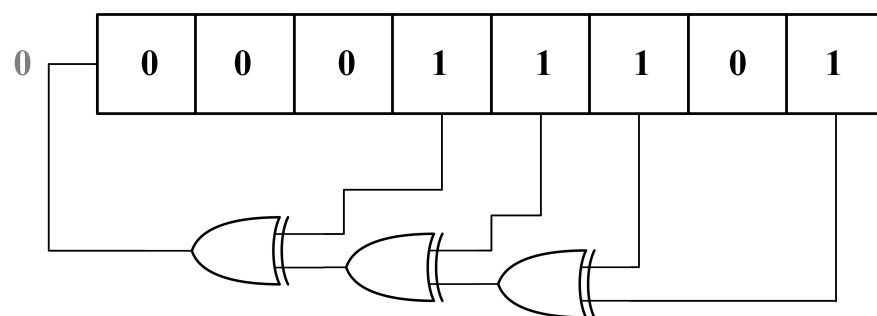

Figure 13. An 8-bit Fibonacci LFSR.

The generator polynomial of this register is shown in Equation (8). The positions of the register bits whose initial states are '1' constitute the polynomial coefficients other than 0.

$$x^8 + x^6 + x^5 + x^4 + 1 = 0 \tag{8}$$

The values generated by the LFSR are stored in a ROM, and then read during the test. The LFSR states with values from 237 to 255 will not produce any change in the matrix of 236 LEDs. Moreover, the visible states depend on the patient-stimulus distance, because for 50 cm only a maximum amount of 118 LEDs is used, while for 100 cm, 236 LEDs are used.

The circumstances mentioned above are considered in the storage of RSAC signal. The SG has a ROM for storing these signal positions, where the states exceeding the 237th value are dismissed for a test where D = 100 cm. If a test is being undertaken where D = 50 cm, the 118 central values will only be addressed. To simplify the ROM, addressing the RSAC test will always have a maximum amplitude of ±30°.

4.3. EOG Acquisition Stage

4.3.1. EOG Amplifier

Figure 14 shows the block outline of the EOG amplifier used for the acquisition of the patient's ocular movements. The amplifier has two input channels for acquiring the horizontal ocular movement (R and L) and the vertical eye movement (U and D), respectively.
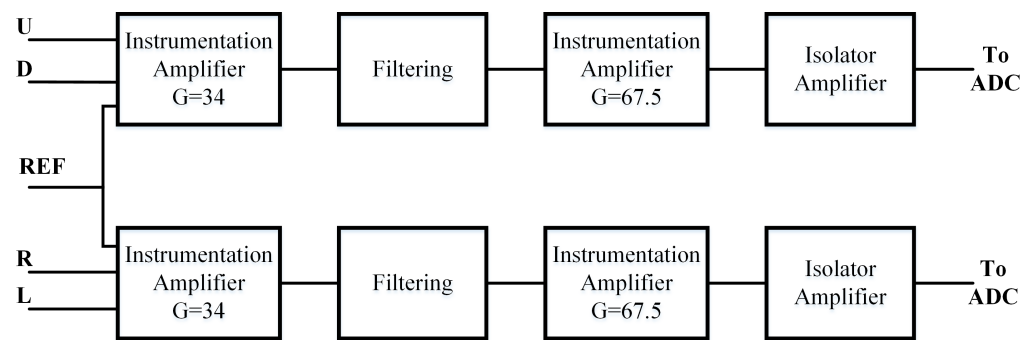
Figure 14. Block Outline of the EOG Amplifier.

As shown in Figure 6, the EOG signal is acquired through five electrodes placed on the patient skin face. According to the ISCEV Standard for Clinical Electrooculography [45], the EOG signal ranges its voltage value from 250 µV to 1000 µV, hence, the signal must be amplified.

As part of the signal conditioning process, two differential amplification stages are incorporated. At the first stage, the main function is to amplify the signal, and the second stage raises the voltage levels, adapting them to the dynamic input range of the Analog-Digital Converter (ADC) used. The first amplification stage should have a low gain, and it is mainly designed to enhance the signal, maintaining its integrity against common mode signals. For this purpose, an instrumentation amplifier could be used. In the second amplification stage, the signal is amplified to obtain the full-scale range of the ADC. An instrumentation amplifier could also be used in this stage.

Between the two amplification stages, there is a filtering process, which is done by three active filters in cascades with a Sallen-Key structure and Butterworth approximation, composed by a high-pass filter (0.05 Hz), a low-pass filter (30 Hz), and a notch suppressor for rejection at 60 Hz. In this stage, the bandwidth is limited to the frequencies that offer useful information about the electro-oculogram, eliminating the rest of the frequencies of other signals or biopotentials that can mask or distort the signal of interest.

The last stage is an Isolator Amplifier to protect the patient from the electrical network. The resulting signal is then sent to an ADC with at least two inputs and a 12-bit output. The ADC also needs to meet the requirements for medical applications. The digitized EOG signal is then sent to the PM block inside the FPGA.

4.3.2. Packaging Module

As it can be seen in Figure 8, the output signal from the multiplexer to the CLI constitutes the stimulus. This signal is also sent to the PM block. In this block, an 8-byte multi-frame is formed, such as the one detailed in Figure 15, which has start and end bytes as delimiters. The second byte gives the status of the stimulus signal, the third one has the EOG channel identification (horizontal or vertical), and the fourth byte gives signaling information related to a misplaced electrode, the battery status, and connection lost. The next three bytes have the EOG signal captured from the patient in response to the visual stimulus. Thus, in the same frame, the FPGA sends the stimulus to the PC and EOG signal, and therefore, temporal and gain parameters can be obtained for the diagnosis of neural diseases.

1 BYTE	1 BYTE	1 BYTE	1 BYTE	1 BYTE	1 BYTE	1 BYTE	1 BYTE
START	STIMULUS	CHANNEL	SIGNALING	EOG RESPONSE	EOG RESPONSE	EOG RESPONSE	END

Figure 15. Multi-frame with the stimulus and EOG signal sent from the FPGA to the fixed station.

4.4. Communication and Power Management Stage

4.4.1. USB Communication

The proposed design uses bidirectional communication protocols for enabling the information exchange with the PC (via USB) and with the rest of the implemented blocks in the FPGA. A USB controller communicates the FPGA with the PC, providing an interface between the 8-bit data port from the FPGA and the USB communication protocol of the PC. The CM module inside the FPGA adapts this protocol for the rest of the SG.

For the communication of $PC \rightarrow FPGA$, a total of four frames are sent containing the characteristics of tests. The first frame contains the information regarding the type of visual stimuli test, its amplitude (α), and the distance D. The second frame provides the characteristics of frequency, while the third and fourth frames signal the orders for beginning and ending the test, respectively. As described in Section 4.3.2, a multi-frame of 8 bytes is sent continuously for the communication $FPGA \rightarrow PC$ while the test is undergoing.

4.4.2. Power Source

The power supply is designed to give the system a certain autonomy of continuous work. The system is designed for working with batteries (12 V/2.7 Ah) and using the power electrical network. To protect the patient and supply the voltages the system needs, an isolated DC-DC converter is used, which receives 12 V and delivers it to voltage regulators that are responsible for supplying power to the whole system.

5. Results

The design evaluation is achieved under the following methodology. The stimuli (digital) amplitude and time domain behavior are verified through the software SignalTap Logic Analizer of the Intel/Altera Quartus tool. A waveform evaluation and a stimulus-response synchronism analysis are also performed. Finally, a general test of the implemented system (Figure 16) is made.

5.1. Description of the Experimental Setup

The main unit behind the system is a DE0 Nano from Intel/Altera Company [46], which obtains a Cyclone IV EP4CE22F17C6 FPGA with 22320 logic elements. The SG, PM and CM are allocated in the FPGA, where the visual stimuli and the processing of the acquired EOG is performed. All these blocks are implemented in VHDL, leading to the overall resource consumption detailed in Table 2.

Table 2. Summary of the FPGA resource usage after placement and routing.

| Resource	Usage	Percentage
Logic elements	9924	44%
Registers	733	3%
LABs	664	48%
Memories 9Ks	3	5%
Total block memories	27,648	5%
Multiplier 9-bits	0	0%

As depicted in Figure 16, the DE0 Nano board interfaces the SP, the EOG amplifier, and the USB controller.

In the SP, the CLI uses two 74,154 integrated circuits (IC) as decoders. These IC are 4- to 16-line decoders, which allows the control of the array of LEDs [47] as a matrix. The outputs of the 74,154 are mutually exclusive and active LOW. The 7404 IC are the inverting gates utilized for converting the LOW logic state from the 74,154 to a HIGH state to light the LEDs through a resistor.

The EOG amplifier designed for acquiring the EOG signal has an overall gain of 2295 V/V (34 V/V in the first stage and 67.5 V/V in the second), to obtain it, two instrumentation amplifiers AD620 [48] are used. The band pass frequency is 0.05 Hz to 30 Hz

with a notch filter in 60 Hz, the operational amplifier used for the filters is the LF412 [49]. The amplifier also has a CMRR = 100 dB, input impedance of 3 MΩ and electrical isolation of 2400 V with the isolation amplifiers ISO124 [50]. The amplifier has two input channels for acquiring the vertical and horizontal ocular movement. Each channel has the same characteristics. Its outputs maximum voltage is 3 V, these output signals are addressed to the serial ADC inputs. The ADC utilized is the 12-bit output ADC128S022 for medical applications localized in the De0 Nano. This converter can work with a clock frequency from 0.8 MHz to 3.2 MHz, hence, its conversion speed can be configured in a variable range from 50 ksps to 200 ksps. The converter is configured to work at 1 MHz clock frequency, which provides a sample rate of 62.5 ksps.

Finally, the UM245R USB-Parallel converter [51] is the USB controller. The stimulus data sent from the FPGA to the PC in sequential 8 bytes multiframes is converted to USB protocol and received by the software in the PC, while the test characteristics are sent to the FPGA via USB and the UM245R convert them into sequential 8-bit frames.
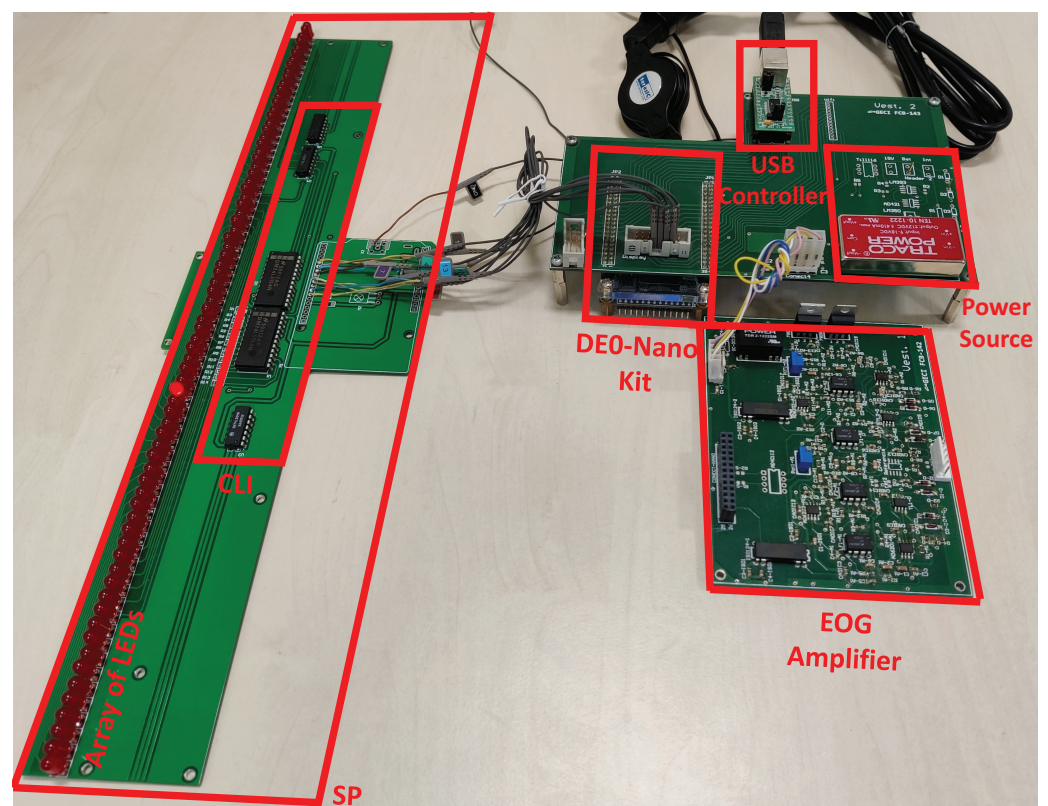
Figure 16. Experimental setup. The principal components are labelled. Only the central part of the array of LEDs is shown. The electrodes for the EOG signal acquisition are not included.

Table 3 summarizes the main components utilized to evaluate the proposed method and system.

Table 3. Components used for implementing the system.

Component(s)	Part ID	Description
CLI	Decoder 74154 [52]	Conversion of the 8 bits signal from the SG to 31 lines for the LEDs stimulation.
	Inverter 7404 [53]	As part of the LEDs stimulation process in the SP.
SG, PM, CM	Intel/Altera DE0-Nano kit [46]	Development board with a Cyclone IV EP4CE22 FPGA.
USB controller	UM245R [51]	USB-Parallel Converter for the communication between the FPGA and the PC.
EOG Acquisition	EOG Amplifier [54]	Amplification of the EOG signal from the patient.
Power Source	DC-DC converters (ISO124 and Traco Power TE 10-1222) [50,55]	Voltage supplier of the system guarantying patient isolation.
	Linear voltage regulators (7805 and 7905) [56,57]	

5.2. Stimuli Generation Analysis

Several tests are done in order to analyze the signals' behavior. Tests include the 12 frequency values and the six amplitude values for both distances. The main aspects to consider are the amplitude, frequency, and the lighting time of each LED. Figures 17–20 show examples of the stimuli signals generated for the four tests.

Figure 17 illustrates a SSAC test for D = 50 cm, an amplitude of ±5° and a frequency of 0.1 Hz. The signal is obtained with SinalTap. The software is configured to obtain four segments of 256 samples of 1 µs each. The sample clock is the PLL output of 1 MHz. Each segment of samples represents the output of the visual stimulator. The output takes the values of 109 (−5°) and 127 (+5°), which is equivalent to switching on LEDs 127 and 109 respectively. The output signal is centered at LED 118 (the center of the SP). The signal *dir* is also visualized, and it indicates the direction of the stimulus. A "high" state of this signal specifies, in this test, that the stimulus is on the left side of the matrix, and a "low" state indicates the stimulus is on the right side.

Figure 18 displays an extract of 8 sets of 128 samples for a SPCS test of 0.5 Hz, ±10° of amplitude for a patient-stimulus distance of 100 cm. In this test, the output signal takes consecutive values, as this is a smooth pursuit test. The *dir* signal indicates the direction of the stimulus, a high state of this signal indicates a left–right direction (as the Figure 18 illustrates), and a low state specifies a right–left movement of the stimulus. The *led_step* signal shows the lighting time (in µs) that each LED has in the test, as this is a SPCS test where all the LEDs have the same lighting time.

Figure 19 illustrates 8 segments of 128 samples of a SPSS test for D = 50 cm, an amplitude of ±20° and 1 Hz of frequency. The output signal behavior is observed. The time duration is different for each output state, and this is the distinctive characteristic of the sinusoidal pattern. Furthermore, the *led_step* signal shows the lighting time (in µs) of each LED, which is higher as the sine wave stimulus reaches their peaks. Additionally, the *dir* signal is in a "low" state, signifying that the stimulus is moving from right to left.

Finally, in Figure 20, a RSAC test can be observed, where the output signal changes its values pseudo-randomly. The test is performed at a frequency of 1.2 Hz for an amplitude of ±30° and a D = 100 cm. The figure shows 8 consecutive segments of 128 samples. The *random_offset* signal addresses the random saccadic ROM with the output signals consecutively.
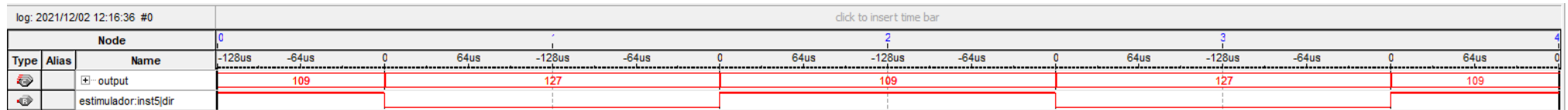
Figure 17. Simulation of a SSAC ±5° and 0.1 Hz stimulus for a 50 cm patient-stimulus distance (-5° = position 109, +5° = position 127).
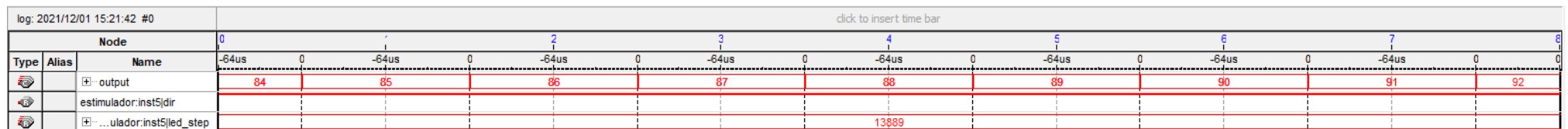

Figure 18. An extract of a period simulation for a SPCS ±10° and 0.5 Hz stimulus for a 100 cm patient-stimulus distance.
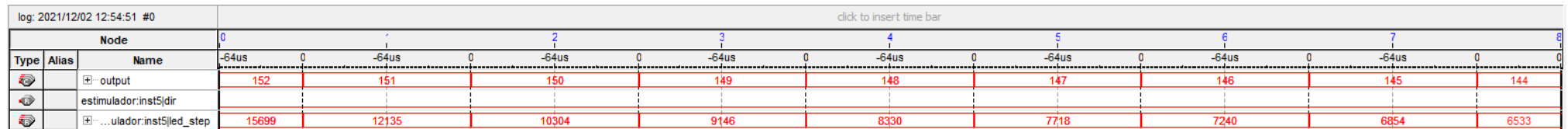

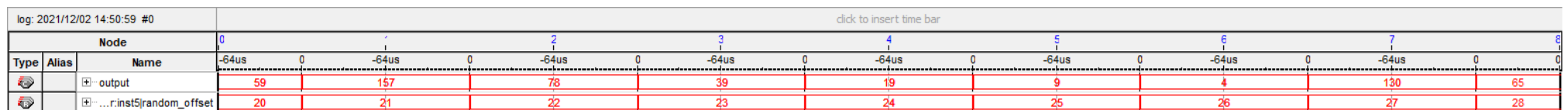**Figure 19.** Simulation of a SPSS ±20° and 1 Hz stimulus for a 50 cm patient-stimulus distance.

Figure 20. Simulation of a RSAC ±30° and 1.2 Hz stimulus for a 100 cm patient-stimulus distance.

5.2.1. Error Analysis

Generating the stimulus signals produces errors in the calculus of LED lighting times, mainly due to the conversion to integers for storing them in ROMs (described in Section 4.2.3). This conversion is done by multiplying the real-time value by the value of the PLL frequency (1 MHz). This error affects all the tests equally, the SPCS and SPSS tests use the same number of LEDs for the same amplitude and frequency, and the SSAC and RSAC use the SPCS signal times for their stimuli generation. For analyzing this error, the SPSS test under the worst working conditions is used.

By multiplying the LED lighting time by a value of 1 MHz, the result obtained represents the number of μs needed to reach this time. The rest of the conversion constitutes the error committed in the test. This is propagated in the generation of the stimulus, and therefore, it increases as the execution time of the tests increases, which is usually 50 s.

The biggest error the visual stimulator makes is in the generation of the stimulus signal at the highest frequency that uses all the LEDs in a period. The signal with an amplitude of ±30° and D = 100 cm uses 236 LEDs of the matrix, therefore, the error committed in the lighting of each LED is propagated 472 times in each period. In a time of 50 s, exactly 60 periods of a stimulus will be counted at a frequency of 1.2 Hz; this is the largest number of periods that can be found for any stimulus.

The period for a 1.2 Hz signal is $833.\overline{3}$ ms. Figure 21 shows the SignalTap simulation for an acquisition of 16 k-samples of an SPSS signal under the conditions mentioned above. The sample clock is 10 kHz. The resolution chosen for the SignalTap time bar is 0.1 ms (clock frequency of 10 kHz), and this allows to visualize a maximum of 1638.4 ms of the stimulus signal. For increasing the resolution of the time bar, it will be necessary to increase the sampling frequency. However, for 100 kHz, only 163.84 ms of the signal could be seen; hence, a period of the stimulus signal cannot be evaluated under these conditions. Therefore, to see a period of $833.\overline{3}$ ms of a signal, the clock frequency of the SignalTap must be, at most, 10 kHz.

Figure 21 shows no errors in the generation of the stimulus, mainly due to the low resolution achieved by the SignalTap. Therefore, the ModelSim software integrated in Quartus is used for evaluating this error more deeply. Figure 22 shows the outcome of the simulation.

Figure 22 shows an error of 0.001 ms for a period of the signal, for which it would be impossible to visualize with the SignalTap. The simulation provides evidence that the visual stimulus is ahead of the theoretical 1.2 Hz sinusoid by 0.001 ms. This represents an error of 0.00012%.

As mentioned before, the duration of a test must be of 50 s. It represents 60 periods of the 1.2 Hz stimulus. Hence, the resulting error would be 0.06 ms for a 50 s stimulus under these conditions. Figure 23 shows the simulation of 60 periods of the stimulus signal on ModelSim.

The end of the 61st period is marked by the red cursor. Hence, the error of the signal generation for the worst-case scenario is approximately 0.073 ms, very close to the theoretical value mentioned above.

This error manifests the phase shift the stimulus signal presents in time regarding its theoretical value. The EOG signal will always be conditioned to the stimulus signal; therefore, the stimulus-response relation is not affected by this error, which has nothing to do with the degree of prediction of the stimulus or the degree of attention of the patient.

5.3. Stimulus-Response Synchronism Evaluation

To guarantee an effective diagnosis of certain neurodegenerative diseases and to perform a suitable analysis in the temporal domain of parameters such as latencies and velocities, it is necessary that the visual stimulus and the EOG signal from the patient are synchronized [5].

The stimulus-response synchronism error is known as the time difference between visual stimulation and the EOG signal acquired from the patient. This error should be

constant (ideally, equal to zero), indicating this process is synchronous, but in practice, there may be some variability.

The EOG signal from a patient must be adequate through several stages of amplification, filtering, and digitization [58]. The last stage causes the greatest delay in the response signal, and therefore affects the synchronism.

The De0 Nano also has the ADC128S022 with 12-bit serial output. The converter is configured to work at a 1 MHz clock frequency, which provides a sample rate of 62.5 ksps. With this configuration, valid data are obtained at the output of the converter every 16 μs, thus the digitization of a sample of the response signal will occur every 16 μs. This time will be the smallest error in synchronism that the stimulus and response signals can have.

This synchronism error is the minimum that can be committed between these signals, and this is because the stimulation and the acquisition of the response signal are two different processes within the FPGA, which only share the same time base (1 μs). Due to its configuration, the ADC provides valid data at its output every 16 clock pulses (in our case every 16 μs); therefore, even in the best-case scenario, in which visual stimulation and acquisition occurs at the same time, there will be a 16 μs delay acquiring the EOG signal from the patient. In the worst-case scenario, the error will be 31 μs, and this occurs when the ADC takes a sample one μs before the stimulus signal changes its value; hence, it is necessary to wait 31 clock pulses in order to see the signal from the ADC in correspondence with the stimulus signal. This, therefore, constitutes the maximum synchronism error of this system. Figure 24 shows the stimulus signal and ADC output signal synchronism for a SPCS signal.

The above allowed us to quantitatively characterize the stimulus-response synchronism error ($16 \text{ μs} < \lambda_{sinc} < 31 \text{ μs}$) of the system. As it can be seen, the limits of this error are quite small when compared with the latency of a healthy person (around 200 ms) or for a SCA2 patient (above 250 ms), both at 30° of the target displacement [19]. Thus, this error does not influence the correct diagnosis.
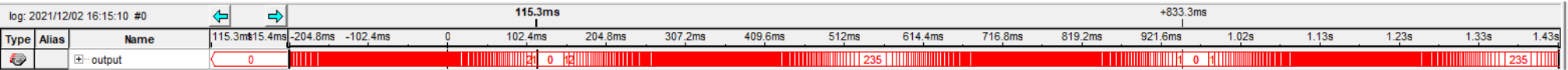
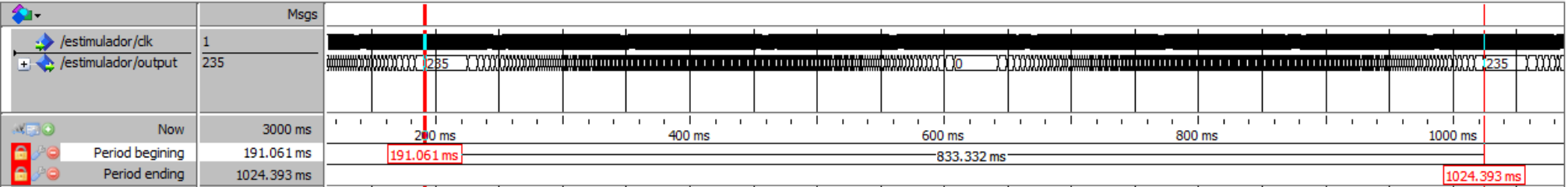**Figure 21.** Segment of 16 k-samples of a SPSS stimulus with amplitude of ±30° at 1.2 Hz with D = 100 cm.

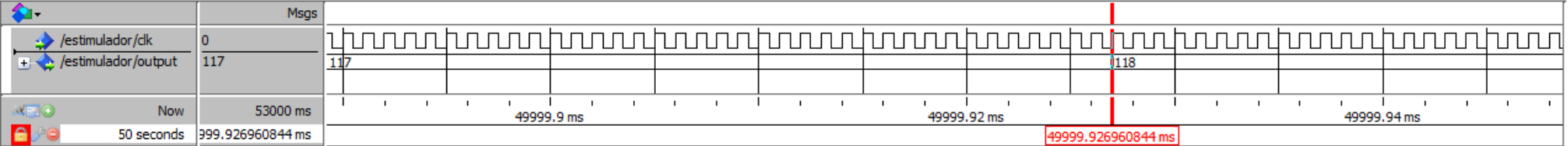**Figure 22.** Error analysis for a SPSS stimulus with amplitude of ±30° at 1.2 Hz with D = 100 cm.

Figure 23. Error analysis for 60 periods of a SPSS signal with ±30° at 1.2 Hz with D = 100 cm.
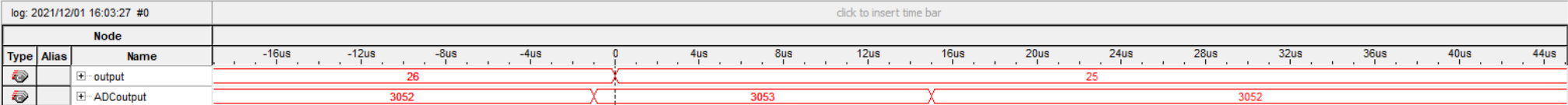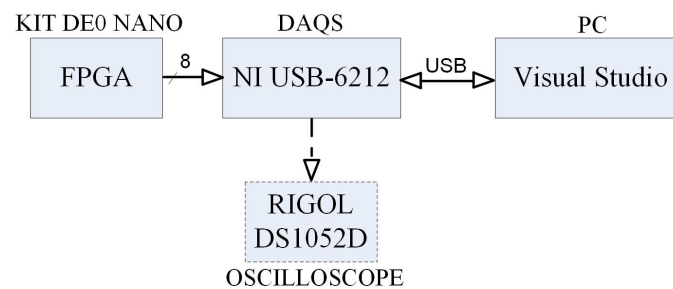

**Figure 24.** Synchronism evaluation for a stimulus signal.

5.4. Evaluation of the Hardware Implementation

Figure 25 indicates the blocks outline of the experimental installation realized to evaluate the stimulator.

Figure 25. Blocks outline of the experimental installation.

The first evaluation consists of acquiring the generated stimulus with the DAQS (8-bit digital signal) through a port of the De0 Nano. This signal is sent to the computer via a USB, where in the PC, its time behavior is visualized. The software designed in the Visual Studio (VS) also calculates the input signal frequency as well as its maximum and minimum values, having as the measure unit the stimulus amplitude in LEDs (A_N). The second experimental test consist of converting the signal acquired in the VS to analog and forward it toward an oscilloscope RIGOL to be visualized. Figure 26 displays four screenshots taken of the oscilloscope for some stimulus signals: (a) RSAC ±30° at 0.5 Hz for D = 50 cm, (b) SPSS ±20° at 0.2 Hz for D = 100 cm, (c) SPCS ±5° at 0.1 Hz for D = 50 cm and (d) SSAC ±30° at 1.1 Hz for D = 100 cm.
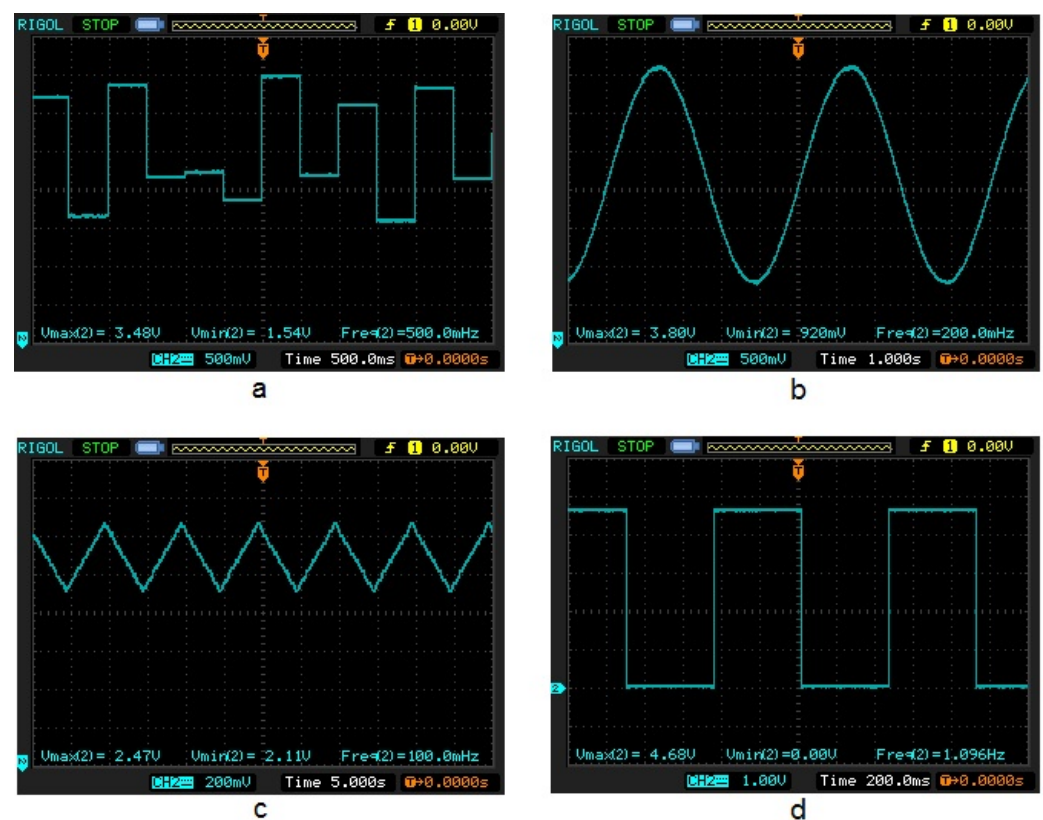
Figure 26. Generated signals viewed on a RIGOL oscilloscope. (**a**) RSAC, (**b**) SPSS, (**c**) SPCS, (**d**) SSAC.

These tests corroborate the results obtained by means of calculation and design. Furthermore, the oscilloscope allows for real-time monitoring of the behavior of the stimulus

signal, its amplitude (in this case represented in volts) and its frequency, as well as other temporary characteristics, like duty cycle, period, rise time, and so forth.

5.5. Waveform Evaluation

The ideal method to analyze the waveform of the generated stimulus signals is to compare each signal with a model, which can be generated in MatLab. Of the four types of stimuli to be analyzed, the one that is most prone to errors is the SPSS signal, because, unlike the SPCS signal, it does not have a linear behavior.

Unlike the smooth pursuit signals, the waveform of the saccades (SSAC and RSAC) is relatively easy to evaluate, because they only have two amplitude states and ideally present discontinuities in the transition between these two states. Therefore, they will not be compared against a pattern. Thus, for the SSAC, RSAC and SPCS signals, the parameters that are considered to analyze their waveform are the rise and fall time, pulse width, duty cycle, DC voltage, and peak values. This evaluation is made through the RIGOL oscilloscope, obtaining satisfactory results. Figure 27 shows the blocks outline used for evaluating the waveform of the SPSS signal.
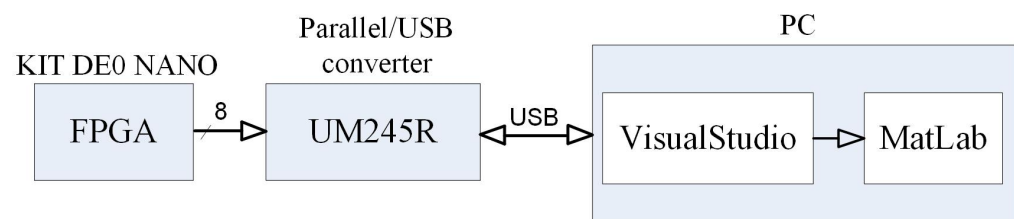
Figure 27. Blocks outline for evaluating the SPSS signal waveform.

The signal delivered by the UM245R to the VS is stored by the software in a file, which is then read in the MatLab and compared with a standard signal.

The parameter chosen to compare both signals is the Root Mean Square Percentage Error (*RMSPE*), which measures the residual or difference between the real signal and the pattern, shown in Equation (9).

$$RMSPE = \left(\sqrt{\frac{\sum_{i=1}^{N}(Y_i - \hat{Y}_i)^2}{\sum_{i=1}^{N} Y_i^2}} \right) \times 100 \text{ \%} \tag{9}$$

where N represents the total samples, Y_i the real value of each sample, and $\hat{Y}_i$, the ideal value each sample should have.

Table 4 shows the results of the RMSPE equation for certain SPSS signals, including the most well-used and the critical cases, which are the signals with periods with several decimals. It demonstrates the similarity between the signals generated and the patterns, and the RMSPE in all cases is below 0.05%.

Table 4. RMSPE results for SPSS signals with certain patient-stimulus distance (*D*), number of LEDS (*A_N*), stimulus amplitude (*A_G*) and frequency (*F_S*).

D (cm)	A_G (°)	A_N (*LED*)	F_S (Hz)	*RMSPE* (%)
50	±5	18	0.1	0.0095
100	±5	36	1.1	0.0231
50	±5	18	0.9	0.0175
50	±15	54	1.0	0.022
100	±20	144	0.2	0.012
100	±25	188	0.5	0.0186
50	±30	118	0.6	0.0362
50	±30	118	0.4	0.0143
100	±30	236	1.2	0.0426

6. Discussion

The tests applied to the system at the software and hardware level, by analyzing the signals generated in real time within the FPGA as well as their behavior in the array of LEDs, demonstrate the correct behavior of the proposed system. The use of an FPGA provides the processing speed and storage capacities for the generation of stimuli along with the synchronous acquisition of the EOG signal. Similarly, the evaluations performed on the rest of the system showed its reliability.

The generated signals differ by little from the ideal signals, with a maximum error of 0.04% obtained in the RMSPE calculations, evidencing the precision of the system. The error in the generation of the stimuli did not exceed 0.073 ms in tests of 50 s for the worst-case scenario, indicating the robustness and accuracy of the SG within the FPGA. Furthermore, the latency in the stimulus-response synchronization is very low compared to that of healthy patients or those suffering from neurodegenerative diseases, being more than 1000 times lower, which means that its influence may be negligible in the clinical parameters of EOG tests.

6.1. System Flexibility

The designed system can be modified in further revisions or extensions. The method designed grants the generation of new stimuli with minor changes in software and without modifying the hardware.

The ramp stimulus (where the signal is a saw-tooth), used for the diagnosis of vestibular diseases, can be easily incorporated into the system. The same values from the t_{SPCS} stimulus can be used for this test. Similarly, a variant of the RSAC test can be designed, in which instead of the amplitude, it is the frequency that takes pseudo-random values. To generate this stimulus, the amplitude values from the SSAC test can be used, where it would only be necessary to control the lit time of each LED, which would cause the pseudo-randomness of the stimulus frequency. These two modifications would not imply an excessive consumption of FPGA resources, since they use resources already implemented in the current tests.

Additionally, the system is also flexible to add other stimulation distances, which should be below 100 cm. It would only imply recalculating the tables of the LED lighting times and their positions in the panel, which is done in the Start condition of our method. On the other hand, implementing the system for a distance greater than 100 cm would imply increasing the size of the LED panel, which in the author's opinion could be unmanageable and bulky.

6.2. Comparison with Other Systems in the Literature

As stated in Section 2, most of the systems found in the literature are closed commercial systems [20,21] and, for copyright reasons, do not provide detailed information on their methods and designs. Research using these type of systems are tied to their specifications [24,26,27], thus they cannot perform a deep evaluation of the stimulus generation and EOG synchronous acquisition and the signal design methodology. Furthermore, visual stimulators implemented by other research groups have not been conceived for the analysis of neurodegenerative diseases through eye movements. The authors have only found the work presented in the Ref. [15], which implements a visual stimulation system based on the Arduino platform for the diagnosis of diseases that affect the CNS.

Our system uses the advantages of hardware parallelism and architecture flexibility of FPGAs to guarantee the stability of the stimulus signals, as well as their synchronism with the response EOG signal coming from the patient. In the Ref. [15] they use two microcontrollers to perform this process, which inherently implies unwanted delays or lack of synchronism. Furthermore, in the cited research, the authors do not perform a deep evaluation of the stimulus signal generation and their characteristics.

The detailed proposed method for generating the stimulus signals grants that our system could be easily reconfigurable, with multiple stimulus generation and the ability to

generate new custom stimuli. The systems described in the literature and the commercial systems do not have this property, which gives our system a great advantage over those previously mentioned.

7. Conclusions

In this work, a novel FPGA-based visual stimulator for the analysis of eye movements towards diagnosis of neurodegenerative diseases was presented. The use of an FPGA allows to obtain high stability in the stimulus signals. The parallel processing of the FPGA architecture enables a high stimulus-response synchronism, which leads to reliable calculations of diagnosis parameters in the time and frequency domain. Furthermore, it outperforms similar systems described in the literature, especially in the analysis of stimulus-response latency, which is an important index for the diagnosis of neurodegenerative diseases. Moreover, unlike the commercial devices, this system is flexible for future extensions or modifications in stimulus signal generation, which grants its use for the diagnosis, through visual stimulation, of other diseases.

Author Contributions: Conceptualization, A.B.F., C.R.V.-S. and B.N.S.H.; methodology, A.B.F., C.R.V.-S. and B.d.S.; software, A.B.F. and J.M.H.R.; validation, A.B.F., B.d.S. and J.M.H.R.; formal analysis, A.B.F., B.d.S. and C.R.V.-S.; investigation, A.B.F. and C.R.V.-S.; resources, B.N.S.H. and B.d.S.; data curation, A.B.F. and B.d.S.; writing—original draft preparation, A.B.F.; writing—review and editing, B.d.S. and C.R.V.-S.; visualization, A.B.F.; supervision, C.R.V.-S. and B.N.S.H.; project administration, C.R.V.-S. and B.N.S.H.; funding acquisition, A.B.F. All authors have read and agreed to the published version of the manuscript.

References

1. Barea, R.; Boquete, L.; Mazo, M.; López, E. System for assisted mobility using eye movements based on electrooculography. *IEEE Trans. Neural Syst. Rehabil. Eng.* **2002**, *10*, 209–218. [CrossRef] [PubMed]
2. CR, H.; MP, P. Classification of eye movements using electrooculography and neural networks. *Int. J. Hum. Comput. Interact. (IJHCI)* **2014**, *5*, 51.
3. Hernández, B.N.S.; Domínguez, D.C.; Regueiro-Gómez, A. Caracterización de Reflejos Vestibulo-Oculares Mediante Electro-Oculografía. Available online: https://www.researchgate.net/profile/Angel-Regueiro-Gomez/publication/311510869_CARACTERIZACION_DE_REFLEJOS_VESTIBULO-OCULARES_MEDIANTE_ELECTRO-OCULOGRAFIA/links/5849890308ae82313e7105b8/CARACTERIZACION-DE-REFLEJOS-VESTIBULO-OCULARES-MEDIANTE-ELECTRO-OCULOGRAFIA.pdf (accessed on 14 December 2021).
4. Ranjbaran, M.; Smith, H.L.; Galiana, H.L. Automatic classification of the vestibulo-ocular reflex nystagmus: Integration of data clustering and system identification. *IEEE Trans. Biomed. Eng.* **2015**, *63*, 850–858. [CrossRef] [PubMed]
5. Rodríguez-Labrada, R.; Velázquez-Pérez, L.; Auburger, G.; Ziemann, U.; Canales-Ochoa, N.; Medrano-Montero, J.; Vázquez-Mojena, Y.; González-Zaldivar, Y. Spinocerebellar ataxia type 2: Measures of saccade changes improve power for clinical trials. *Mov. Disord.* **2016**, *31*, 570–578. [CrossRef]
6. Terao, Y.; Fukuda, H.; Hikosaka, O. What do eye movements tell us about patients with neurological disorders?—An introduction to saccade recording in the clinical setting. *Proc. Jpn. Acad. Ser. B* **2017**, *93*, 772–801. [CrossRef] [PubMed]
7. Netto, A.A.T.d.C.; Colafêmina, J.F. Movimentos sacádicos em indivíduos com alterações cerebelares. *Braz. J. Otorhinolaryngol.* **2010**, *76*, 51–58. [CrossRef]
8. Pinzón-Amado, A.; León-Martínez, N.E.; Blanco-Díaz, M.J. Asociación entre la alteración de los movimientos oculares sacádicos y la esquizofrenia: Un estudio de casos y controles. *Rev. Colomb. Psiquiatr.* **2007**, *36*, 628.
9. Ettinger, U.; Picchioni, M.; Hall, M.H.; Schulze, K.; Toulopoulou, T.; Landau, S.; Crawford, T.J.; Murray, R.M. Antisaccade performance in monozygotic twins discordant for schizophrenia: The Maudsley twin study. *Am. J. Psychiatry* **2006**, *163*, 543–545. [CrossRef]

10. Van der Geest, J.N.; Kemner, C.; Camfferman, G.; Verbaten, M.N.; van Engeland, H. Eye movements, visual attention, and autism: A saccadic reaction time study using the gap and overlap paradigm. *Biol. Psychiatry* **2001**, *50*, 614–619. [CrossRef]

11. Bylsma, F.W.; Rasmusson, D.X.; Rebok, G.W.; Keyl, P.M.; Tune, L.; Brandt, J. Changes in visual fixation and saccadic eye movements in Alzheimer's disease. *Int. J. Psychophysiol.* **1995**, *19*, 33–40. [CrossRef]

12. Moss, H.E.; McCluskey, L.; Elman, L.; Hoskins, K.; Talman, L.; Grossman, M.; Balcer, L.J.; Galetta, S.L.; Liu, G.T. Cross-sectional evaluation of clinical neuro-ophthalmic abnormalities in an amyotrophic lateral sclerosis population. *J. Neurol. Sci.* **2012**, *314*, 97–101. [CrossRef] [PubMed]

13. Kanayama, R.; Nakamura, T.; Sano, R.; Ohki, M.; Okuyama, T.; Kimura, Y.; Koike, Y. Effect of aging on smooth pursuit eye movement. *Acta Oto-Laryngol.* **1994**, *114*, 131–134. [CrossRef] [PubMed]

14. Griffiths, A.; Marshall, R.; Richens, A. Saccadic eye movement analysis as a measure of drug effects on human psychomotor performance. *Br. J. Clin. Pharmacol.* **1984**, *18*, 73S–82S. [CrossRef] [PubMed]

15. Pérez Guzmán, R.E.; Céspedes Pérez, A.; García Bermúdez, R.V.; Pérez Céspedes, A. Estimulador visual y auditivo para pruebas clínicas de electrooculografía basado en la plataforma Arduino. *Rev. Cuba. Cienc. Informáticas* **2017**, *11*, 77–91.

16. Oliveira, W.M.; Viana, N.L.; Brito-Filho, F.A. Sistema Automatizado Baseado em FPGA para Eletro-Oculograma Clínico. In *Revista Ibérica de Sistemas e Tecnologias de Informação*; Associacao Iberica de Sistemas e Tecnologias de Informacao (AISTI)': Lousada, Portugal, 2020; pp. 272–285.

17. Srivastava, A.; Sharma, R.; Sood, S.K.; Shukla, G.; Goyal, V.; Behari, M. Saccadic eye movements in Parkinson's disease. *Indian J. Ophthalmol.* **2014**, *62*, 538.

18. Ohki, M.; Kanayama, R.; Nakamura, T.; Okuyama, T.; Kimura, Y.; Koike, Y. Ocular abnormalities in amyotrophic lateral sclerosis. *Acta Oto-Laryngol.* **1994**, *114*, 138–142. [CrossRef] [PubMed]

19. Rodríguez-Labrada, R.; Velázquez-Pérez, L.; Seigfried, C.; Canales-Ochoa, N.; Auburger, G.; Medrano-Montero, J.; Sánchez-Cruz, G.; Aguilera-Rodríguez, R.; Laffita-Mesa, J.; Vázquez-Mojena, Y.; et al. Saccadic latency is prolonged in Spinocerebellar Ataxia type 2 and correlates with the frontal-executive dysfunctions. *J. Neurol. Sci.* **2011**, *306*, 103–107. [CrossRef]

20. DI 14050X-ENGU: Ideas III ENG DIFRA. Available online: https://www.difra.be/shop/product/00022315-di-14050x-engu-ideas-iii-eng-19217?category=4 (accessed on 14 December 2021).

21. Gladius201 PC Based ENG machine General Medical Inc. Available online: https://www.generalmedicalinc.in/diagnostic-product.html#rms-gladius-201-pc-based-eng-machine (accessed on 14 December 2021).

22. Orban de Xivry, J.J.; Bennett, S.J.; Lefèvre, P.; Barnes, G.R. Evidence for synergy between saccades and smooth pursuit during transient target disappearance. *J. Neurophysiol.* **2006**, *95*, 418–427. [CrossRef]

23. Daye, P.M.; Blohm, G.; Lefèvre, P. Saccadic compensation for smooth eye and head movements during head-unrestrained two-dimensional tracking. *J. Neurophysiol.* **2010**, *103*, 543–556. [CrossRef]

24. Parisi, V.; Pierelli, F.; Malandrini, A.; Carrera, P.; Olzi, D.; Gregori, D.; Restuccia, R.; Parisi, L.; Fattapposta, F. Visual electrophysiological responses in subjects with cerebral autosomal arteriopathy with subcortical infarcts and leukoencephalopathy (CADASIL). *Clin. Neurophysiol.* **2000**, *111*, 1582–1588. [CrossRef]

25. Chabriat, H.; Joutel, A.; Dichgans, M.; Tournier-Lasserve, E.; Bousser, M.G. Cadasil. *Lancet Neurol.* **2009**, *8*, 643–653. [CrossRef]

26. Ettinger, U.; Kumari, V.; Crawford, T.J.; Corr, P.J.; Das, M.; Zachariah, E.; Hughes, C.; Sumich, A.L.; Rabe-Hesketh, S.; Sharma, T. Smooth pursuit and antisaccade eye movements in siblings discordant for schizophrenia. *J. Psychiatr. Res.* **2004**, *38*, 177–184. [CrossRef]

27. Zhai, X.; Enderle, J.D. Visually Guided Horizontal Saccades under the Double-Step Paradigm. *J. Biomed. Eng. Med. Devices* **2016**, *113*, 1–7. [CrossRef]

28. Da Silva Pinto, M.A.; de Souza, J.K.S.; Baron, J.; Tierra-Criollo, C.J. A low-cost, portable, micro-controlled device for multi-channel LED visual stimulation. *J. Neurosci. Methods* **2011**, *197*, 82–91. [CrossRef]

29. Sun, Y.; Zhao, L.; Xu, N.; Ou, R. Research of Visual Stimulation Method and Design of Visual Stimulator Based on Brain-Computer Interface. Applied Mechanics and Materials. *Trans. Tech. Publ.* **2015**, *734*, 375–382.

30. Xie, S.; Wang, L.; Obermayer, K.; Zhu, F. Design of Visual Stimulation System with LED in the Study of Spatial Selective Attention. In *Advances in Cognitive Neurodynamics (V)*; Springer: Sanya, China, 2016; pp. 461–468.

31. Svilainis, L. Comparison of the EMI performance of LED PWM dimming techniques for LED video display application. *J. Disp. Technol.* **2012**, *8*, 162–165. [CrossRef]

32. Albeanu, D.F.; Soucy, E.; Sato, T.F.; Meister, M.; Murthy, V.N. LED arrays as cost effective and efficient light sources for widefield microscopy. *PLoS ONE* **2008**, *3*, e2146. [CrossRef] [PubMed]

33. Fadraga, Y. Métodos y Herramientas para el Análisis de los Movimientos Oculares de Persecución Lenta Utilizando el MEDICID 4.0. Tesis de Maestría, Universidad de Oriente', Santiago de Cuba, Cuba, 2015.

34. Bermúdez, R.V.G. Procesamiento de registros oculares sacádicos en pacientes de ataxia SCA2. Aplicación del Análisis de Componentes Independientes. In *Universidad de Granada*; 2010. Available online: https://dialnet.unirioja.es/servlet/cittes?codigo=63105 (accessed on 14 December 2021)

35. Gallego Navarrete, D. Desarrollo de un Sistema de Adquisición y Procesado de Señales Electrooculográficas para el Diagnóstico de la Ataxia. 2007. Available online: https://www.recercat.cat/handle/2072/6517 (accessed on 14 December 2021).

36. Zhai, X.; Enderle, J.D. Horizontal Saccadic Eye Movements to Visual and Auditory-Visual Double-Step Stimuli: Saccade Characteristics and Neural Input Estimations. *J. Biomed. Eng. Med. Devices* **2016**, *1*, 1–5.

37. Robinson, D.A. The mechanics of human smooth pursuit eye movement. *J. Physiol.* **1965**, *180*, 569–591. [CrossRef]
38. Van Steveninck, A.L.; Schoemaker, H.C.; Pieters, M.S.; Kroon, R.; Breimer, D.D.; Cohen, A.F. A comparison of the sensitivities of adaptive tracking, eye movement analysis, and visual analog lines to the effects of incremental doses of temazepam in healthy volunteers. *Clin. Pharmacol. Ther.* **1991**, *50*, 172–180. [CrossRef]
39. Wessel, K.; Moschner, C.; Wandinger, K.P.; Kömpf, D.; Heide, W. Oculomotor testing in the differential diagnosis of degenerative ataxic disorders. *Arch. Neurol.* **1998**, *55*, 949–956. [CrossRef]
40. Lindsey, D.T.; Holzman, P.S.; Haberman, S.; Yasillo, N.J. Smooth-pursuit eye movements: A comparison of two measurement techniques for studying schizophrenia. *J. Abnorm. Psychol.* **1978**, *87*, 491. [CrossRef] [PubMed]
41. Rottach, K.G.; Zivotofsky, A.Z.; Das, V.E.; Averbuch-Heller, L.; Discenna, A.O.; Poonyathalang, A.; Leigh, R.J. Comparison of horizontal, vertical and diagonal smooth pursuit eye movements in normal human subjects. *Vis. Res.* **1996**, *36*, 2189–2195. [CrossRef]
42. Collewijn, H.; Tamminga, E.P. Human smooth and saccadic eye movements during voluntary pursuit of different target motions on different backgrounds. *J. Physiol.* **1984**, *351*, 217–250. [CrossRef] [PubMed]
43. Parra, M.A. Método para el estudio de los movimientos oculares. *Colomb. Médica* **2004**, *35*, 55–61.
44. Szirmai, A.; Keller, B. Electronystagmographic analysis of optokinetic and smooth pursuit eye movement disorders in vestibular lesions. *Int. Tinnitus J.* **2011**, *16*, 1–15.
45. Constable, P.A.; Bach, M.; Frishman, L.J.; Jeffrey, B.G.; Robson, A.G. ISCEV Standard for clinical electro-oculography (2017 update). *Doc. Ophthalmol.* **2017**, *134*, 1–9. [CrossRef] [PubMed]
46. De0 Nano User Manual Altera. Available online: https://www.terasic.com.tw/cgi-bin/page/archive.pl?Language=English&No=593&PartNo=4 (accessed on 14 December 2021).
47. TLHR540., TLHY540., TLHG540. High Efficiency LED, Ø 5 mm Tinted Diffused Package Vishay Electronics. Available online: https://www.mouser.be/datasheet/2/427/VISH_S_A0009750987_1-2570663.pdf (accessed on 14 December 2021).
48. Low Cost, Low Power Instrumentation Amplifier. AD620 Analog Devices. Available online: https://www.analog.com/media/en/technical-documentation/data-sheets/AD620.pdf (accessed on 14 December 2021).
49. LF412 Low Offset, Low Drift Dual JFET Input Operational Amplifier National Semiconductor. Available online: https://pdf1.alldatasheet.com/datasheet-pdf/view/462294/TI1/LF412.html (accessed on 14 December 2021).
50. ISO124 Precision Lowest-Cost Isolation Amplifier Texas Instruments. Available online: https://www.ti.com/lit/ds/symlink/iso124.pdf?ts=1639520540447&ref_url=https%253A%252F%252Fwww.google.com%252F (accessed on 14 December 2021).
51. UM245R USB—Parallel FIFO Development Module Datasheet Future Technology Devices International Ltd. Available online: https://ftdichip.com/wp-content/uploads/2020/08/DS_UM245R.pdf (accessed on 14 December 2021).
52. DM74LS154 4-Line to 16-Line Decoder/Demultiplexer Fairchild Semiconductors. Available online: https://pdf1.alldatasheet.es/datasheet-pdf/view/51037/FAIRCHILD/DM74LS154N.html (accessed on 14 December 2021).
53. DM74LS04 Hex Inverting Gates Fairchild Semiconductors. Available online: https://pdf1.alldatasheet.com/datasheet-pdf/view/51022/FAIRCHILD/74LS04.html (accessed on 14 December 2021).
54. Hernandez, B.N.S. Sistema Automatizado Para la Detección de Enfermedades Vestibulares Basado en el Analisis Espectro-Temporal de Nistagmogramas. Ph.D. Thesis, Universidad Tecnológica de la Habana Jose Antonio Echeverria, La Habana, Cuba, 2018.
55. DC/DC Converters Ten 10 Series 10 Watt Traco Power. Available online: https://www.tracopower.com/sites/default/files/products/datasheets/ten10_datasheet.pdf (accessed on 14 December 2021).
56. LM340, LM340A and LM78xx Wide V_IN 1.5-A Fixed Voltage Regulators Texas Instruments. Available online: https://pdf1.alldatasheet.com/datasheet-pdf/view/838007/TI1/LM7805.html (accessed on 14 December 2021).
57. LM79XX Series 3-Terminal Negative Regulators Texas Instruments. Available online: https://www.ti.com/lit/ds/snosbq7c/snosbq7c.pdf?ts=1599268479365 (accessed on 14 December 2021).
58. López, A.; Ferrero, F.; Villar, J.R.; Postolache, O. High-performance analog front-end for EOG systems. *Electronics* **2020**, *9*, 970. [CrossRef]